NASA TN D-2005

TECHNICAL NOTE

D-2005

THE EFFECT OF INITIAL IMPERFECTIONS ON THE BUCKLING STRESS OF CYLINDRICAL SHELLS

By C. D. Babcock and E. E. Sechler

Prepared under Grant No. NsG-18-59 by
CALIFORNIA INSTITUTE OF TECHNOLOGY
Pasadena, California

for

NATIONAL AERONAUTICS AND SPACE ADMINISTRATION
WASHINGTON

July 1963

NATIONAL AERONAUTICS AND SPACE ADMINISTRATION

TECHNICAL NOTE D-2005

THE EFFECT OF INITIAL IMPERFECTIONS ON THE BUCKLING STRESS OF CYLINDRICAL SHELLS

by C. D. Babcock and E. E. Sechler

California Institute of Technology

SUMMARY

An experimental investigation is carried out to determine the effect of an axially symmetric initial imperfection on the buckling load of a circular cylindrical shell under axial compression loading. The imperfection studied has the form of a half sine wave in the length direction. The shells are formed by a copper electroforming process. The theoretical buckling loads are also computed for the imperfect shells, and show the same trend as the experimental study.

INTRODUCTION

The large discrepancy between the classical buckling load of a circular cylindrical shell under axial compression and the experimental values of the buckling load is a well known but little understood phenomenon (Ref. 1). Several reasons for this discrepancy have been proposed but have yet to be substantiated by adequate experimental investigations. Donnell and Wan (Refs. 2 and 3) have shown that imperfections in geometrical shape have an important effect but the exact degree of this effect for various types of imperfections is still to be determined. The idea of a jump of the shell from the prebuckled state at a load lower than the classical load has been proposed by von Kármán and Tsien (Refs. 4 and 5) but the exact mechanism of the jump and conditions under which it is possible are as yet unexplored.

The purpose of this investigation was to study the effect of a specific type of initial imperfection under very carefully controlled conditions. In order to accomplish this the following steps have been carried out:

1. development of a method of making cylindrical shells which were as nearly perfect as possible:

2. establishment of testing techniques in which the stress distribution was controllable and measurable:

3. determination of the buckling stress of these nearly perfect shells:

4. addition of the initial imperfections to be studied and the determination of the buckling stress.

The investigation was conducted at the Graduate Aeronautical Laboratories of the California Institute of Technology under the sponsorship and financial assistance of the National Aeronautics and Space Administration, Research Grant NsG-18-59.

LIST OF SYMBOLS

a_o	Amplitude of initial imperfection in inches
a_1	$a_o 2\sqrt{3(1-\nu^2)}/t$
A_j	Eigenvector of buckling problem
A_{ij}, B_{ij}	General coefficients of eigenvalue problem
a_{mj}, b_{ij}, c_{ij} d_{mj}, e_{mj}, f_{mj} g_{mj}, h_{mj} k_{mj+1}, k_{mj-1}	Constants defined on page 17
C_1, C_2, C_3, C_4	Constants defined on page 16
D	$Et^3/12(1-\nu^2)$
E	Young's modulus
$F, F^*, \overline{F}$	Stress function
K	$\frac{\sigma_o R}{Et}$

L	Length of shell
m, $\bar{m}$	Circumferential wave number
N_x, N_y, N_{xy}	Membrane stresses for shallow shell equations
n	Axial wave number
R	Base radius of shells
t	Shell thickness
$u, \bar{u}, u^*$	Axial deflection of shell
$v, \bar{v}, v^*$	Circumferential deflection of shell
$w, w^*, \bar{w}$	Radial deflection of shell
w_o	Initial distance of shell from flat plate
x	Axial coordinate
y	Circumferential coordinate
$\Gamma_1, \Gamma_2, \Gamma_3, \Gamma_4$	Constants defined on page 16
δ_{ij}	Kronecker delta
$\zeta, \bar{\zeta}$	x variation of radial deflection
$\eta, \bar{\eta}$	x variation of stress function
λ	$-\frac{\sigma_o R}{Et} 2\sqrt{3(1-\nu^2)}$
ν	Poisson's ratio
ξ	$\pi x/L$

σ_o Applied axial stress

σ_{cl} $\dfrac{1}{3(1-\nu^2)}\dfrac{Et}{R}$

∇^4 $\left(\dfrac{\partial^2}{\partial x^2}+\dfrac{\partial^2}{\partial x^2}\right)^2$

EXPERIMENTAL INVESTIGATION

Fabrication of the Test Specimens

The method of manufacturing of the cylindrical shells is not new with GALCIT (see reference 6) but a number of refinements were required in order to obtain the uniformity and accuracy desired. Basically it consisted of plating a copper shell on an accurately machined wax mandrel and then melting the mandrel out of the shell. For a shell 8 inches in diameter and 10 inches long, a steel cylinder 7 inches in diameter and 13 inches long was used as a core (this provided a means of water cooling the wax to harden it). On this core was cast a layer of wax consisting of a two to one mixture of refined paraffin and Mobile Cerese Wax 2305. This was cooled, machined to the proper shape, and sprayed with silver paint thinned with toluene. Figure 1 shows a mandrel and finished wax form. The plating was done in a Cupric Fluoborate, $Cu(BF_4)_2$, bath with a 15 inch diameter copper anode which was bagged in fine mesh Dynel fabric. During plating the mandrel was rotated and the bath was given additional agitation by forcing air through it. Using voltages less than 10 volts and current densities up to 55 amperes per square foot, the plating time was approximately 20 minutes per 0.001 inches of plate.

After plating, the ends of the cylinder were removed (some thickness increase occurred just at the ends), the wax was carefully melted out, and the residual wax and silver paint was removed with benzene. The shell thickness used in this series of tests was approximately 0.0045 inches. The thickness variation in any shell could be held to less than 3 per cent. In the radial direction, the desired radius could be held to $\pm$ t/2 or approximately $\pm$ 0.0025 inches.

Tests to determine the characteristics of the plated copper were carried out in uniaxial tension. This was done by utilizing long strips of the copper that were soldered into one-eighth inch thick plates that were in turn clamped into the jaws of an Instron testing machine. The strips had length to width ratios greater than 15. The head displacement of the testing machine was used as the measure of strain and the load was read from the Instron load cell. A typical stress-strain curve is shown in Figure 2. The value of Young's modulus used in this work was 13.0×10^6 lb/in^2.

A determination of Poisson's ratio was not attempted since its influence in the reduction of the buckling data is of secondary importance. A value of 0.30 was used for this purpose.

Test Procedure

The buckling tests were carried out in the controlled displacement testing machine shown in Figure 3. This machine was designed to be rigid in comparison with the test specimen and capable of subjecting the test cylinder to very small increments of end displacement. The relative displacement of the two end plates of the testing machine was controlled by three screws. One complete turn of the screws gave a displacement of 0.025 inches. The screws could be operated independently to give the proper load distribution on the shell and then simultaneously to increase the load to the buckling point. The springs shown in the figure were used to preload the testing machine when mounting the test specimen in the machine and securing it to the end plate of the testing machine. The testing was carried out when the machine was in the position shown in Figure 3. The end plate with the gear drive rested on pins and the opposite end rested on a set of rollers.

The load distribution was monitored and total load was obtained on the load measuring cylinder shown in Figures 4 and 5. This consisted of a seamless brass cylinder which was 0.0107 inches thick, 2.5 inches long and 8.000 inches in diameter. Twenty-four foil-type strain gauges were mounted on the cylinder equally spaced around the circumference. The ones on the inside were directly opposite to those on the outside.

In order to see if the strain being measured in the load measuring cylinder corresponded to the strain in the test shell, the following test was carried out. A test cylinder was instrumented with strain gauges that were located at every other circumferential position as those on the load measuring cylinder. The test shell was mounted in the load

measuring cylinder and both sets of gauges read as the shell was eccentrically loaded. Two typical readings showing the correspondence of the measured strains are shown in Figure 6.

The test cylinder was cast with a low melting temperature alloy into an end ring and the other end was secured to the load measuring cylinder in the same manner. After this operation was completed the shell was measured to determine the initial imperfection.

In this series of tests the initial imperfection that was measured was the deviation of the generators of the shell from a straight line. This measurement was carried out at nine stations around the circumference. The measurements were made with a reluctance type pick up which has a sensitivity of about 25 volts per inch. The noise level and drift were such that deflection of 10^{-4} inches could be accurately read without making contact with the measured surface

The measurements were carried out by mounting the sensing head of the pick up in a slide which traveled on a guide. The guide was attached to the end rings of the shell to be measured and readings were taken at 32 stations along the generator. The pick up and guide are shown in Figure 7.

After the initial imperfections were measured, the end ring was then secured to the end plate of the testing machine with a thin layer of Devcon. After hardening of the Devcon was complete, the cylinder was ready for testing.

The buckling test was carried out in the following manner. The cylinder was initially loaded to about one-third of the expected buckling load, and the circumferential load distribution was made as uniform as possible by adjusting the three screws of the testing machine. The load was then gradually increased in small increments by turning the three screws simultaneously. After each increase the load distribution was adjusted again. This was carried out up to about two-thirds of the expected buckling load. After this point the load distribution was not adjusted so as to prevent buckling occurring during one of the adjustments. The load was increased in small increments and the strain gauges monitored until buckling occurred.

Test Results

Two types of axially symmetric imperfections were tested in this series of tests. Thirty-seven shells with an initial deformation of the form $\Delta R = a_o \sin \pi x/L$ were buckled and three with an imperfection of constant curvature given by $\Delta R = a_o \{2(2x/L) - (2x/L)^2\}$ were also tested. Table I shows the intended imperfection of the shells and Figures 8 through 16 give the measured imperfection on several of the shells. These figures show the shell generator at nine locations equally spaced around the circumference. Table I also shows the wall thickness of the shell tested. All shells had a base diameter of 8 inches and a length of 10 inches.

Table I shows that some of the shells had an initial buckling. This initial buckling consisted of the formation of one wave on the surface of the shell. This caused the load distribution to fall off in the neighborhood of the one wave without appreciably affecting the distribution over the rest of the circumference of the shell. After the initial buckling, the load was increased until general collapse occurred without attempting to alter the load distribution. General collapse occurred in the same manner as for the shells that did not have an initial buckling.

General collapse consisted of a snap-through which is characteristic of this type of testing. In all but a few cases the post-buckled state consisted of 2 to 3 rows of buckles that extended completely around the circumference. The number of circumferential waves is noted in Table I. All of the shells that had an initial imperfection amplitude greater than 0.010 inches buckled at one end or the other. This buckled state consisted of 2 to 3 rows of buckles that started quite close to one end and extended about one-third of the way up the shell. There did not seem to be a preferred end for this buckling to take place. The other shells with small positive imperfection, negative imperfection, and no intended imperfection buckled over the middle third of the shell. Again this consisted of 2 to 3 rows that extended completely around the circumference.

Table I also gives the maximum variation in load distribution near buckling. The average maximum variation in load distribution for all the shells tested was 18.6 per cent. In most cases the average stress was nearer the maximum stress rather than the minimum. Figures 17 and 18 show the load distribution on two shells as the load was increased. The initial buckling is easily detected in Figure 18. Figures 19 and 20 give the load distribution on several of the other shells at the last reading before buckling.

The values of K for this series of tests are given in Table I and the values of σ_{cr}/σ_{cl} are plotted versus a_o/t in Figure 21. These are compared with the Kanemitsu and Nojima value which for the L/R and R/t corresponding to these specimens gives K = 0.17. The theoretical curve shown in the figure is the result of the analysis given in the Appendix. The following important features can be seen:

1. That with proper care in manufacturing and testing, values of the buckling stresses can be obtained which are much higher than those usually found.

2. That, for the displacement forms tested, small departures from initial straightness lower the buckling stress and that the effect for inward displacements is greater than that for outward displacements.

3. That if the outward displacements are increased the value of the buckling stress again rises until it reaches essentially the same value as that for the initially straight cylinder.

4. That the constant curvature and sine wave shape give essentially the same values of σ_{cr} for the larger values of a_o/t.

The drop in the value of σ_{cr} for $0 < a_o/t < 10$ and the return to the "perfect" value for $a_o/t > 20$ cannot be explained at this time. It is felt that some of the scatter in the experimental results can be accounted for by the variation of stress around the circumference of the shells. Also the lowering of the value of σ_{cr} below the classical value may be in part due to the fact that the classical buckling load, as well as that computed in the Appendix, is calculated under the assumption that the shell is free to expand in the radial direction during the loading while the edges of the test cylinders were rigidly clamped.

APPENDIX

DETERMINATION OF BUCKLING LOADS FOR A CYLINDRICAL SHELL WITH AN AXIAL SYMMETRIC IMPERFECTION HAVING THE SHAPE OF A HALF SINE WAVE IN THE LENGTH DIRECTION

The method of solution is as follows:

1. Determine the stresses and deflections in the shell that occur before buckling during the loading.

2. Consider the stresses and deflections occurring during the buckling as small perturbations about the solution of step 1 and linearize the equations.

3. Solve the eigenvalue problem obtained in 2 and determine the smallest eigenvalue.

The equations that will be used for the solution are the shallow shell equations of Marguerre (Ref. 7). Using the coordinate system shown in figure 22, the equations are:

$$\nabla^4 F = Et\left\{w_{xy}^2 - w_{xx}w_{yy} + 2w_{oxy}w_{xy} - w_{oxx}w_{yy} - w_{xx}w_{oyy}\right\} \tag{1a}$$

$$D\nabla^4 w = F_{yy}(w_{xx} + w_{oxx}) - 2F_{xy}(w_{xy} + w_{oxy}) + F_{xx}(w_{yy} + w_{oyy}) \tag{1b}$$

where w_o is the initial deviation from the flat plate and F is the stress function defined as:

$$\frac{\partial^2 F}{\partial x^2} = N_y, \qquad \frac{\partial^2 F}{\partial y^2} = N_x, \qquad \frac{\partial^2 F}{\partial x \partial y} = -N_{xy}, \tag{2}$$

and

$$w_{xx} = \frac{\partial^2 w}{\partial x^2}, \quad F_{xx} = \frac{\partial^2 F}{\partial x^2} \text{ etc.}$$

Equation 1a is a compatibility relation and equation 1b is the equilibrium equation in the direction perpendicular to the xy plane.

In the case of interest here as shown in Figure 22:

$$w_o = \frac{1}{2R}(y^2 - y^2_o) - a_o \sin \frac{\pi x}{L} . \tag{3}$$

Let F^*, and w^* be the solutions of the axial symmetric problem before the buckling occurs. Let $\bar{F}$ and $\bar{w}$ be the perturbation stress function and radial deflection occurring during the buckling. Then

$$F = F^* + \bar{F} \qquad w = w^* + \bar{w}. \tag{4}$$

Substituting Equation 3 and 4 into Equation 1 and remembering that the * state is axially symmetric, one obtains:

$$\underline{\nabla^4 F^* + \frac{Et}{R} w^*_{xx}} + \nabla^4 \bar{F} + Et\left\{\bar{w}_{yy}(w^*_{xx} + a_o (\tfrac{\pi}{L})^2 \sin \tfrac{\pi x}{L}) + \right.$$

$$\left. + \frac{1}{R}\bar{w}_{xx}\right\} + Et\left\{\bar{w}_{xx}\bar{w}_{yy} - \bar{w}_{xy}^2\right\} = 0,$$

$$\underline{D\frac{d^4 w^*}{dx^4} - F^*_{yy}(w^*_{xx} + a_o(\tfrac{\pi}{L})^2 \sin \tfrac{\pi x}{L}) - F^*_{xx}\frac{1}{R}} + D\nabla^4 \bar{w} + \tag{5}$$

$$- \bar{F}_{yy}(w^*_{xx} + a_o(\tfrac{\pi}{L})^2 \sin \tfrac{\pi x}{L}) - F^*_{yy}\bar{w}_{xx} - \bar{F}_{xx}\frac{1}{R} - F^*_{xx}\bar{w}_{yy} +$$

$$+ \left\{- \bar{F}_{yy}\bar{w}_{xx} + 2\bar{F}_{xy}\bar{w}_{xy} - \bar{F}_{xx}\bar{w}_{yy}\right\} = 0.$$

Since F^* and w^* are the solutions for the pre-buckled state, the terms that are underlined are equal to zero. Also, since we are only

interested in the bifurcation points of the solutions, the perturbations may be considered arbitrarily small and all nonlinear terms in $\bar{F}$ and $\bar{w}$ can be dropped. This leaves us with the following set of equations:

$$\nabla^4 \bar{F} = Et \left\{ - \bar{w}_{yy} (w^*_{xx} + a_o (\tfrac{\pi}{L})^2 \sin \tfrac{\pi x}{L}) - \frac{1}{R} \bar{w}_{xx} \right\}$$

$$D \nabla^4 \bar{w} = \bar{F}_{yy} (w^*_{xx} + a_o (\tfrac{\pi}{L})^2 \sin \tfrac{\pi x}{L}) + F^*_{yy} \bar{w}_{xx} + \bar{F}_{xx} \frac{1}{R} + F^*_{xx} \bar{w}_{yy}, \tag{6}$$

which is seen to have a solution of the form:

$$\bar{w} = \bar{\xi}(x) \sin \frac{\bar{m} y}{R}, \qquad \bar{F} = \bar{\eta}(x) \sin \frac{\bar{m} y}{R}. \tag{7}$$

This solution satisfies the necessary periodic conditions in the circumferential direction when $\bar{m}$ is a whole number.

Axially Symmetric Solution

The axially symmetric solution must satisfy the following set of equations:

$$\nabla^4 F^* + \frac{Et}{R} w^*_{xx} = 0 \tag{8a}$$

$$D \frac{d^4 w^*}{dx^4} - F^*_{yy} (w^*_{xx} + a_o (\tfrac{\pi}{L})^2 \sin \tfrac{\pi x}{L}) - \frac{1}{R} F^*_{xx} = 0 \tag{8b}$$

It will be assumed that the shell is free to expand radially at the ends during the loading and that the edges of the shell are supported in a pinned manner as the shell expands radially. This expansion is due to the Poisson ratio and is equal to $\frac{\nu R \sigma_o}{E}$, where σ_o is the applied stress.

Therefore, the boundary conditions on w^* are as follows:

$$w^* - \frac{\nu R\sigma_o}{E} = 0, \quad w^*_{xx} = 0 \quad \text{at} \quad x = 0, L \tag{9}$$

The boundary conditions on F^* are given by:

$$F^*_{yy} = N_x = \sigma_o t \quad \text{at} \quad x = 0, L \tag{10}$$

The other conditions necessary to completely specify the problem are that u^* and w^* must be independent of y and that v^* must be identically zero.

Using these conditions the solution of the axially symmetric problem is given by:

$$w^* = \frac{\nu R\sigma_o}{E} + \frac{\sigma_o t\, a_o (\frac{\pi}{L})^2}{D(\frac{\pi}{L})^4 + \sigma_o\, t(\frac{\pi}{L})^2 + \frac{Et}{R^2}} \sin\frac{\pi x}{L} \tag{11}$$

$$F^* = \frac{1}{2}\,\sigma_o\, t\, y^2 + \frac{\sigma_o t\, a_o}{D(\frac{\pi}{L})^4 + \sigma_o t(\frac{\pi}{L})^2 + \frac{Et}{R^2}} \frac{Et}{R} \sin\frac{\pi x}{L} .$$

The denominator $D(\frac{\pi}{L})^4 + \sigma_o t(\frac{\pi}{L})^2 + \frac{Et}{R^2}$ can be written in the following form:

$$(\frac{\pi}{L})^2 \frac{Et^2}{2R\sqrt{3(1-\nu^2)}} \left\{ \frac{Rt}{2\sqrt{3(1-\nu^2)}} (\frac{\pi}{L})^2 + \frac{\sigma_o{}^2 \sqrt{3(1-\nu^2)}R}{Et} + \frac{2\sqrt{3(1-\nu^2)}}{Rt} (\frac{L}{\pi})^2 \right\} \tag{12}$$

The middle term is equal to two when σ_o is the classical buckling stress and the first and last terms are reciprocals of each other. The value of the last term, for the shells that were tested in the experimental part of this work, is 1832. Since the σ_o of interest is always of the order of the classical buckling stress the denominator can be approximately rewritten as Et/R^2. Therefore, the quantities of interest, which occur in the perturbation equations, can be written as:

$$w^*_{xx} = \frac{\sigma_o}{E} R^2 a_o \left(\frac{\pi}{L}\right)^4 \sin \frac{\pi x}{L},$$

$$F^*_{xx} = -\sigma_o Rt \, a_o \left(\frac{\pi}{L}\right)^2 \sin \frac{\pi x}{L}, \tag{13}$$

$$F^*_{yy} = \sigma_o t.$$

It is noticed that w^*_{xx} occurs in the coefficient of the perturbation equations always in combination with $a_o(\pi/L)^2 \sin \frac{\pi x}{L}$. Therefore, this coefficient can be written as:

$$a_o \left(\frac{\pi}{L}\right)^2 \sin \frac{\pi x}{L} \left\{1 - \frac{\sigma_o}{E} \left(\frac{R\pi}{L}\right)^2\right\} \tag{14}$$

For the shells of concern here, R is of the order of L and σ_o is much less than E. Therefore, this second term in the brackets can be neglected in comparison with one. This amounts to neglecting the additional curvature of the shell in the x-direction caused by the loading in comparison with the initial curvature of the shell in this direction.

Solution of the Perturbation Equations

After the initial load is applied, the ends of the shell are assumed to be pinned with respect to the radial direction. This implies

$$\overline{w} = \frac{\partial^2 \overline{w}}{\partial x^2} = 0 \qquad \text{at } x = 0, L$$

or since

$$\overline{w} = \overline{\varphi} \sin \frac{\overline{m} y}{R}$$

$$\overline{\varphi} = \overline{\varphi}'' = 0 \quad \text{at} \quad x = 0, L \tag{15}$$

The boundary conditions that will be applied on $\overline{F}$ are as follows:

$$\overline{F} = \frac{\partial^2 \overline{F}}{\partial x^2} = 0, \quad \text{at } x = 0, L$$

or since

$$\overline{F} = \overline{\eta} \sin \frac{\overline{m} y}{R}$$

$$\overline{\eta} = \overline{\eta}'' = 0 \quad \text{at } x = 0, L \tag{16}$$

These conditions on $\overline{F}$ imply that at the ends of the shell the stress in the axial direction and $\overline{v}$ are equal to zero.

These boundary conditions are commonly used in shell stability analyses because of their simplicity. They can be looked upon as allowing the ends of the shell to warp freely in the axial direction, constraining the circumferential movement, and giving a pinned support with respect to the radial direction.

Now let us introduce the nondimensional quantities as follows:

$$\varphi = \overline{\varphi}/t, \quad \eta = \overline{\eta} \frac{2\sqrt{3(1-\nu^2)}}{Et^3}, \quad \xi = x\frac{\pi}{L}, \quad m = \overline{m}\frac{L}{\pi R}$$

$$a_1 = \frac{a_o 2\sqrt{3(1-\nu^2)}}{t}, \quad a = \frac{2\sqrt{3(1-\nu^2)}}{Rt}\left(\frac{L}{\pi}\right)^2, \quad \lambda = -\frac{\sigma_o R}{Et} 2\sqrt{3(1-\nu^2)}. \tag{17}$$

Using equations 13 and 17 the perturbation equations given by equation 6 become:

$$\eta^{IV} - 2m^2\,\eta'' + m^4\eta = -a\,\zeta'' + a_1 m^2 \zeta \sin\xi \tag{18}$$

$$\zeta^{IV} - 2m^2\,\zeta'' + m^4\zeta = -\lambda a\,\zeta'' + a\eta'' - \lambda a_1 m^2 \zeta \sin\xi - a_1 m^2 \eta \sin\xi.$$

where: $\eta' = \frac{d\eta}{d\xi}$ etc.

The solution given here will be an approximate one which satisfies the compatibility equation exactly and the equilibrium equation approximately. The procedure is as follows.

1. Assume a suitable form of ζ which contains a number of arbitrary constants and satisfies exactly the necessary boundary conditions.

2. Substitute ζ into the compatibility equation and solve for η making sure that η satisfies all the necessary boundary conditions.

3. Substitute ζ and η obtained in the first two steps in the equilibrium equation and determine the unknown constants in such a manner so as to minimize the error by the Galerkin method.

It is assumed that ζ can be represented by the following series which satisfies the necessary boundary conditions:

$$\zeta = \sum_{j=1}^{n} A_j \sin j\xi. \tag{19}$$

Solving the compatibility equation for η gives

$$\eta = \sum_{j=1}^{n} \frac{a_j^2}{a_{mj}} A_j \sin j\xi + \frac{a_1 m^2}{2} \sum_{j=1}^{n} A_j \left\{ \frac{\cos(j-1)\xi}{a_{mj-1}} - \frac{\cos(j+1)\xi}{a_{mj+1}} \right\} \tag{20}$$

$$+ C_1 \sinh m\xi + C_2 \cosh m\xi + C_3 \xi \sinh m\xi + C_4 \xi \cosh m\xi,$$

where C_1 to C_4 must be determined in such a manner that the boundary conditions are satisfied. This gives the following values for C_1 to C_4.

$$C_1 = \frac{1}{2m \sinh^2 m\pi} \left\{ \Gamma_1 (2m \cosh m\pi \sinh m\pi + m^2\pi) - \Gamma_2 \pi + \right.$$

$$\left. + \Gamma_3 (-2m \sinh m\pi - m^2 \pi \cosh m\pi) + \Gamma_4 \pi \cosh m\pi \right\}$$

$$C_2 = -\Gamma_1$$

$$C_3 = \frac{1}{2m} \left\{ m^2 \Gamma_1 - \Gamma_2 \right\} \tag{21}$$

$$C_4 = \frac{1}{2m \sinh m\pi} \left\{ -\Gamma_1 m^2 \cosh m\pi + \Gamma_2 \cosh m\pi + \Gamma_3 m^2 - \Gamma_4 \right\}$$

where

$$\Gamma_1 = \frac{a_1 m^2}{2} \sum_{j=1}^{n} A_j \left\{ \frac{1}{a_{mj-1}} - \frac{1}{a_{mj+1}} \right\}, \Gamma_2 = -\frac{a_1 m^2}{2} \sum_{j=1}^{n} A_j \left\{ \frac{(j-1)^2}{a_{mj-1}} - \frac{(j+1)^2}{a_{mj+1}} \right\}$$

$$\Gamma_3 = \frac{a_1 m^2}{2} \sum_{j=1}^{n} A_j (-1)^{j-1} \left\{ \frac{1}{a_{mj-1}} - \frac{1}{a_{mj+1}} \right\}, \Gamma_4 = -\frac{a_1 m^2}{2} \sum_{j=1}^{n} A_j (-1)^{j-1} \left\{ \frac{(j-1)^2}{a_{mj-1}} - \frac{(j+1)^2}{a_{mj+1}} \right\}.$$

Next ζ and η are substituted in the equilibrium equation which is written in the following manner:

$$\zeta^{IV} - 2m^2\zeta'' + m^4\zeta + \lambda a\zeta'' - a\eta'' + \lambda a_1 m^2 \zeta \sin\xi + a_1 m^2 \eta \sin\xi = \overline{E}. \qquad (22)$$

$\overline{E}$ represents the error resulting from the fact that this equation is not identically satisfied. The unknown constants are determined by a Galerkin procedure in the following manner:

$$\int_0^{\pi} \overline{E} \sin i\xi \, d\xi = 0, \qquad i = 1, 2, \ldots n. \qquad (23)$$

The resulting equations for the A_j's then become:

$$\sum_{j=1}^{n} (A_{ij} - \lambda B_{ij}) A_j = 0 \qquad i, j \text{ both even or odd}, \qquad (24)$$

where

$$B_{ij} = \delta_{ij} - (b_{ij} - c_{ij}) \frac{a_1 m^2}{a\pi i^2}$$

$$A_{ij} = \left\{ \frac{a_{mj}}{a_j^2} + \frac{a_j^2}{a_{mj}} + \frac{a_1 m^4}{4a_j^2} f_{mj} \right\} \delta_{ij} + \frac{a_1 m^2}{\pi i^2} \left\{ b_{ij} k_{mj-1} - c_{ij} k_{mj+1} \right\} +$$

$$- \frac{a_1^2 m^4}{4a\, i^2} \left\{ \delta_{i,j-2} \frac{1}{a_{mj-1}} - \delta_{i,2-j} \frac{1}{a_{mj-1}} + \delta_{i,j+2} \frac{1}{a_{mj+1}} \right\} +$$

$$+ \frac{2a_1 m^2}{\pi i} \left\{ \frac{m^2 g_{mj}}{a_{mi}} - \frac{e_{mj}}{\sqrt{a_{mi}}} \right\} + \frac{a_1^2 m^3}{2\pi a i^2} \left\{ g_{mj} h_{mi} - 2m^2 d_{mj} g_{mi} \right\}$$

$$a_{mj} = (m^2 + j^2)^2, \quad b_{ij} = \frac{1}{i+j-1} + \frac{1}{i-j+1}, \quad c_{ij} = \frac{1}{i+j+1} + \frac{1}{i-j-1}$$

$$d_{mj} = \frac{1}{a_{mj-1}} - \frac{1}{a_{mj+1}}, \quad e_{mj} = \frac{(j-1)^2}{a_{mj-1}} - \frac{(j+1)^2}{a_{mj+1}}, \quad f_{mj} = \frac{1}{a_{mj+1}} + \frac{1}{a_{mj-1}}$$

$$g_{mj} = \frac{1}{\sqrt{a_{mj-1}}} - \frac{1}{\sqrt{a_{mj+1}}}, \quad h_{mj} = e_{mj} - m^2 d_{mj}$$

$$k_{mj-1} = \frac{j^2}{a_{mj}} + \frac{(j-1)^2}{a_{mj-1}}, \quad k_{mj+1} = \frac{j^2}{a_{mj}} + \frac{(j+1)^2}{a_{mj+1}}$$

The minimum eigenvalue will be dependent on the number of circumferential waves m as well as the parameters of the problem a_1 and a which are the amplitude of the initial imperfection and the properties of the shell. The solutions of the eigenvalue problem were found by using an IBM 7090 digital computer.

In all the calculations carried out the parameter containing the shell dimensions was fixed at the value corresponding to the experimental test cylinders. This value of a was 1832. Both the even and odd problems were computed. The results of this calculation for five values of $a_1 < 0$ are shown in Figure 23. The classical value for the perfect shell corresponds to 1. The numbers on the curves correspond to the predominant term in the eigenvector.

The absolute minimum eigenvalue over the whole range of the circumferential wave number is easily found from these curves as well as the corresponding circumferential wave number. The mode shape of this minimum is seen to be the first mode. This means that the buckling shape for $a_1 < 0$ has the form $\sin \frac{\pi x}{L}$ in the axial direction. The higher modes contribute only about a 2 per cent correction to this pattern. The number of circumferential waves varies from 6 to 8 as a_1 varies from -100 to 0.

In the case where the shell bows outward, meaning $a_1 > 0$, convergence of the eigenvalue problem was not obtained. However, the classical buckling load corresponding to the value of $\lambda = 2$ was established as a lower bound for all values of $a_1 > 0$.

The variation of the theoretical buckling load with a_o/t is shown in Figure 21.

Since for $a_o < 0$ the reduction in buckling load given by the theory is much less than that found in the tests the following comparison was made. The value of the buckling stress was found that corresponded to approximately the same number of waves in the circumferential direction as that found in the tests. The comparison for $a_o < 0$ is shown in Figure 24. The numbers on the curves correspond to the predominant term in the eigenfunction expansion, and those at the ends of the curves to the number of circumferential waves. It is seen that the decrease in buckling stress with increasing negative imperfection amplitude is less as the circumferential wave number increases. The buckling mode shape is also more in line with the experimental results. The eigenfunction has more axial waves as the number of circumferential waves increases and the amplitude of the waves at the center of the shell is greater than the amplitude of the waves at the edges. Again, this is nearer the experimental results.

REFERENCES

1. Fung, Y. C., and Sechler, E. E.: Instability of Thin Elastic Shells. Structural Mechanics, Proc. of First Symposium on Naval Structural Mechanics, Pergamon Press, 1960.

2. Donnell, L. H.: A New Theory for the Buckling of Thin Cylinders under Axial Compression and Bending. Trans. of the American Soc. of Mech. Eng., vol. 56, November 1934, p. 795.

3. Donnell, L. H., and Wan C. C.: Effect of Imperfections on Buckling of Thin Cylinders and Columns under Axial Compression. Journal Appl. Mech., vol. 17, no. 1, (1950), p. 73.

4. von Kármán, T., and Tsien, H. S.: The Buckling of Thin Cylindrical Shells under Axial Compression. Journal Aero. Sciences, vol. 8, no. 8, June 1941, p. 302.

5. Tsien, H. S.: A Theory for the Buckling of Thin Shells. Journal Aeronautical Sciences, vol. 9, no. 10, August 1942, p. 373.

6. Thompson, J. M. T.: Making of Thin Metal Shells for Model Stress Analysis. Journal Mech. Eng. Sciences, vol. 2, no. 2, 1960.

7. Marguerre, K.: Zur Theorie der gekrummten Platte grosser Formanderung. Proc. 5th International Congress Appl. Mech., 1938, p. 93.

TABLE I

SUMMARY OF BUCKLING TESTS

III = Intended Initial Imperfection, $K = \frac{\sigma_o R}{Et}$, $\bar{m}$ = Number of Circumferential Waves

Shell	III inches	$t \times 10^3$ inches	a_o/t	K initial	K collapse	σ_{cr}/σ_{cl}	$\frac{\sigma_{max} - \sigma_{min}}{\sigma_{ave}}$ %	$\bar{m}$
A	0	4.62	0	-	0.460	0.76	19.4	16-18
B	0	4.45	0	-	0.438	0.72	16.1	14-15
C	0	4.50	0.5	-	0.435	0.72	23.7	15-17
Y	0.010S in $\pi x/L$	4.82	2.1	-	0.429	0.71	14.4	15-17
Z	0.010S in $\pi x/L$	4.61	2.2	-	0.359	0.59	17.1	15
AA	0.010S in $\pi x/L$	4.50	2.2	0.305	0.362	0.60	15.4	16-17
7	0.010S in $\pi x/L$	4.57	4.5	-	0.407	0.67	13.0	14-18
V	0.020S in $\pi x/L$	4.49	4.5	-	0.326	0.54	55.4	16-17
W	0.020S in $\pi x/L$	4.49	4.5	-	0.352	0.58	26.1	14-15
X	0.020S in $\pi x/L$	4.32	4.6	0.258	0.337	0.56	9.7	15
8	0.020S in $\pi x/L$	4.60	4.4	-	0.423	0.70	19.2	15-17
9	0.020S in $\pi x/L$	4.70	4.3	-	0.418	0.69	12.8	22-24
M	0.030S in $\pi x/L$	4.52	6.6	-	0.369	0.61	15.5	19-20

TABLE I (contd.)

SUMMARY OF BUCKLING TESTS

III = Intended Initial Imperfection, $K = \frac{\sigma_o R}{Et}$, $\bar{m}$ = Number of Circumferential Waves

Shell	III inches	$t \times 10^3$ inches	a_o/t	K initial	K collapse	σ_{cr}/σ_{cl}	$\frac{\sigma_{max} - \sigma_{min}}{\sigma \text{ ave}}$ o/o	$\bar{m}$
N	0.030S in $\pi x/L$	4.57	6.6	-	0.342	0.56	18.0	16-17
O	0.030S in $\pi x/L$	4.46	6.7	0.351	0.377	0.62	10.0	21
J	0.040S in $\pi x/L$	4.27	9.4	-	0.366	0.60	21.3	17
K	0.040S in $\pi x/L$	4.57	8.8	-	0.346	0.57	9.7	16-17
L	0.040S in $\pi x/L$	4.46	9.0	0.272	0.321	0.53	16.7	13-15
G	0.050S in $\pi x/L$	4.60	11.1	-	0.297	0.49	19.7	21
H	0.050S in $\pi x/L$	4.46	10.7	-	0.385	0.64	17.3	21-22
I	0.050S in $\pi x/L$	4.68	10.7	-	0.312	0.52	10.9	18-20
2	0.100S in $\pi x/L$	4.36	22.9	0.361	0.369	0.61	15.8	18-20
3	0.100S in $\pi x/L$	4.56	21.9	-	0.416	0.69	12.7	19-20
AB	-0.010S in $\pi x/L$	4.59	-2.2	-	0.398	0.66	9.2	14-15
AC	-0.010S in $\pi x/L$	4.60	-2.2	-	0.423	0.70	22.8	14-16
AD	-0.010S in $\pi x/L$	4.57	-2.2	-	0.333	0.55	28.6	16-18
AE	-0.020S in $\pi x/L$	4.58	-4.4	-	0.292	0.48	21.3	16-18

TABLE I (contd.)

SUMMARY OF BUCKLING TESTS

III = Intended Initial Imperfection, $K = \frac{\sigma_o R}{Et}$, $\bar{m}$ = Number of Circumferential Waves

Shell	III inches	$t \times 10^3$ inches	a_o/t	K initial	K collapse	$\sigma_{cr}/\sigma_{c\ell}$	$\frac{\sigma_{max} - \sigma_{min}}{\sigma \text{ ave}}$ o/o	$\bar{m}$
AF	-0.020S in $\pi x/L$	4.74	-4.2	-	0.281	0.46	14.9	18-20
S	-0.040S in $\pi x/L$	4.50	-8.9	-	0.331	0.55	19.7	15
T	-0.040S in $\pi x/L$	4.50	-8.9	0.271	0.283	0.47	32.5	13-14
U	-0.040S in $\pi x/L$	4.61	-8.7	-	0.267	0.44	22.3	13
4	-0.040S in $\pi x/L$	4.53	-8.8	-	0.373	0.62	19.9	14-16
5	-0.040S in $\pi x/L$	4.49	-8.9	-	0.316	0.52	14.6	14-16
P	-0.050S in $\pi x/L$	4.45	-10.7	-	0.267	0.44	11.7	14
Q	-0.050S in $\pi x/L$	4.51	-11.1	0.258	0.268	0.44	20.0	14
R	-0.050S in $\pi x/L$	4.42	-10.9	0.231	0.308	0.51	14.5	15-16
1	-0.050S in $\pi x/L$	4.52	-11.1	-	0.361	0.60	41.9	15
11	$0.100\left\{2\left(\frac{x}{L/2}\right)-\left(\frac{x}{L/2}\right)^2\right\}$	4.49	22.3	-	0.430	0.71	9.7	17-18
12	$0.200\left\{2\left(\frac{x}{L/2}\right)-\left(\frac{x}{L/2}\right)^2\right\}$	4.56	43.8	-	0.437	0.72	12.0	18-19
13	$0.200\left\{2\left(\frac{x}{L/2}\right)-\left(\frac{x}{L/2}\right)^2\right\}$	4.47	44.7	-	0.355	0.59	17.5	19

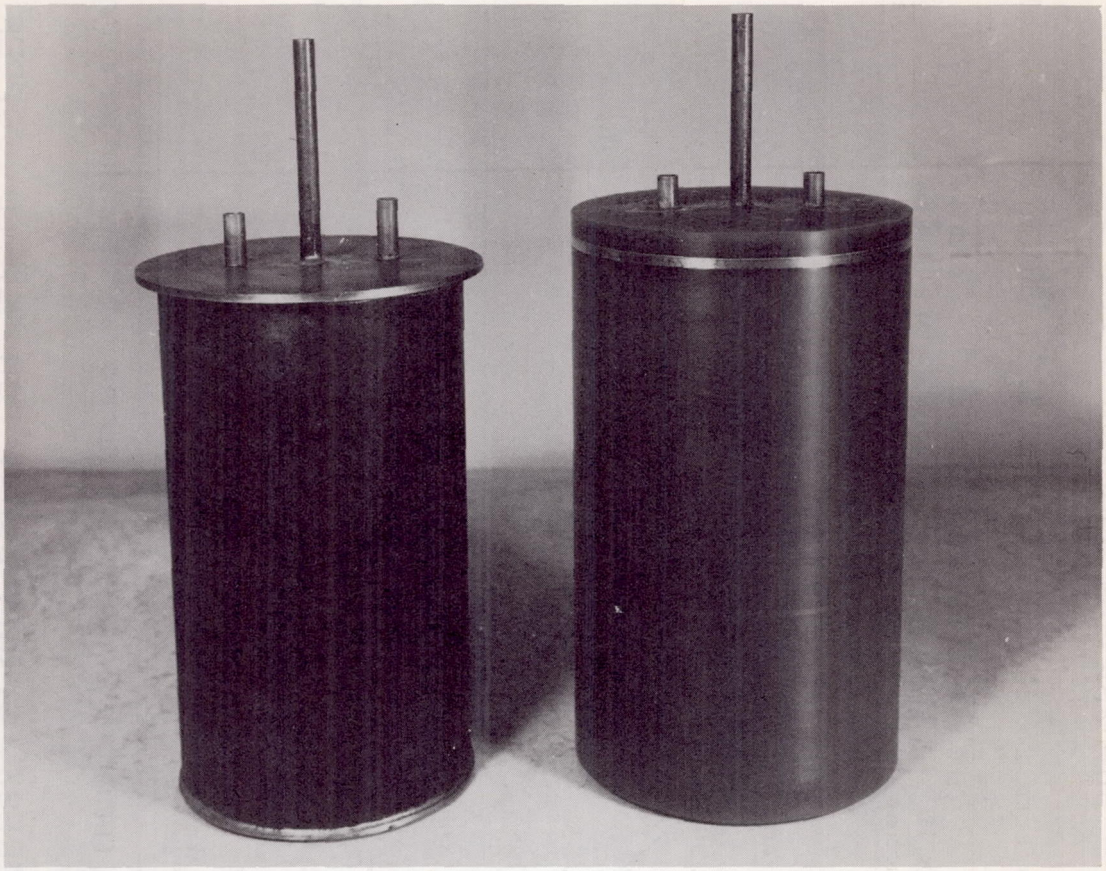

Fig. 1 - Mandrel and Finished Wax Form

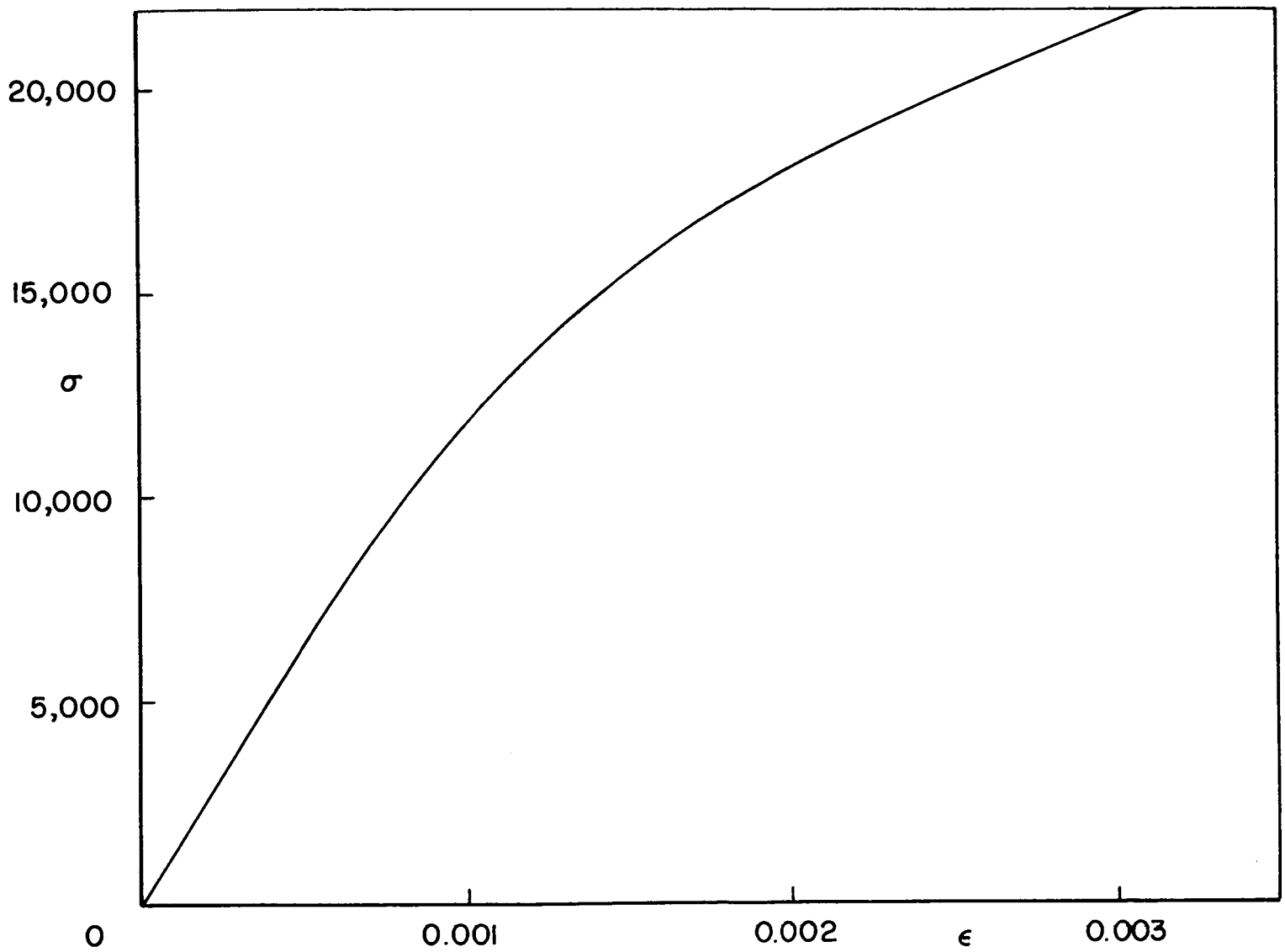

FIG. 2 - STRESS STRAIN CURVE FOR PLATED COPPER

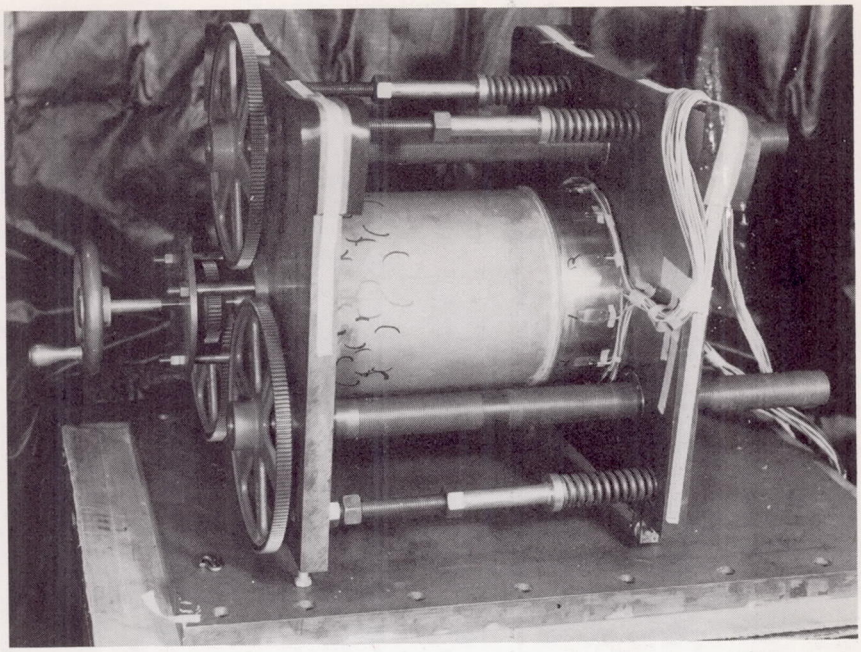

Fig. 3 - Testing Machine

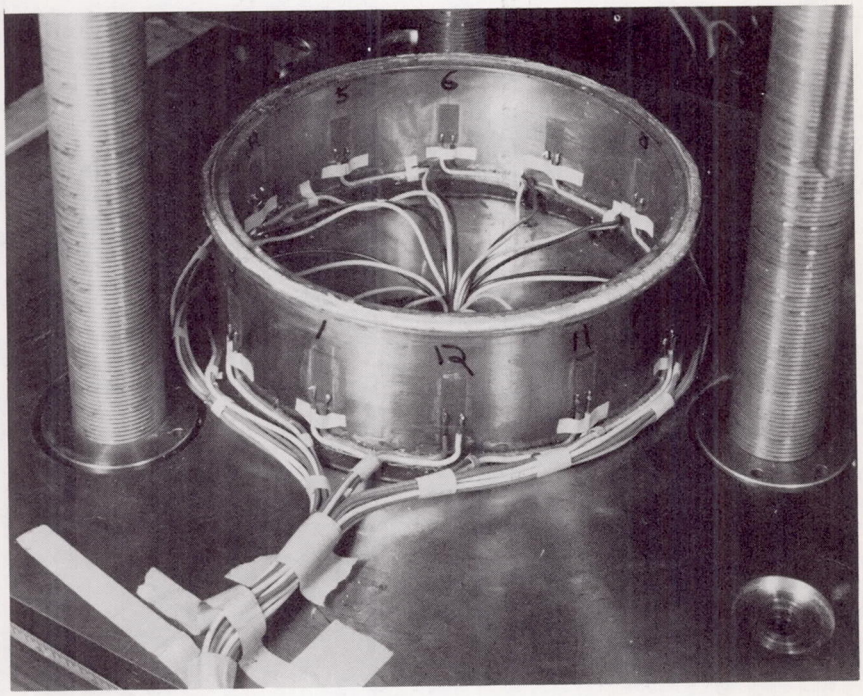

Fig. 4 - Load Measuring Cylinder

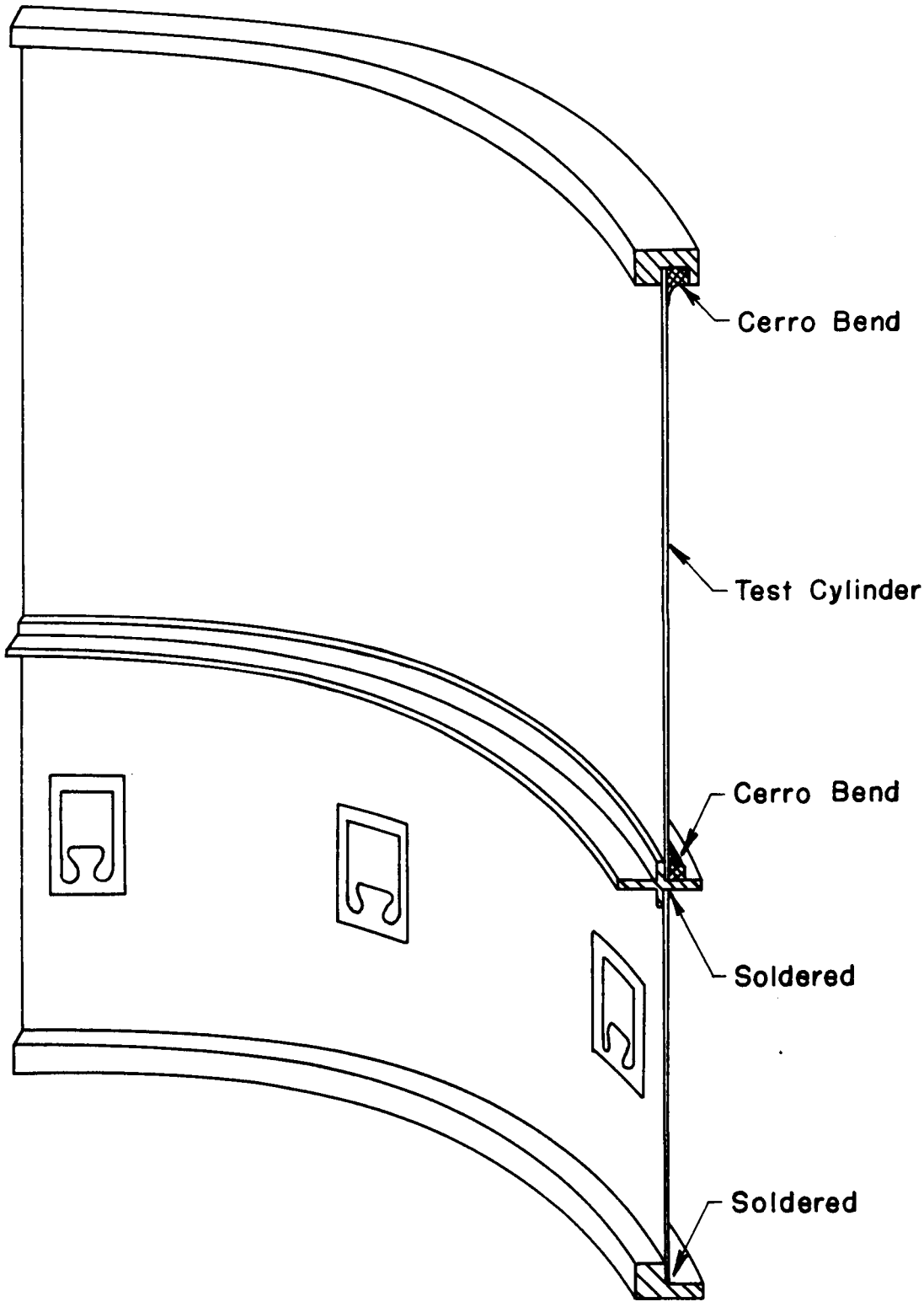

FIG. 5 - DETAILS OF LOAD MEASURING CYLINDER

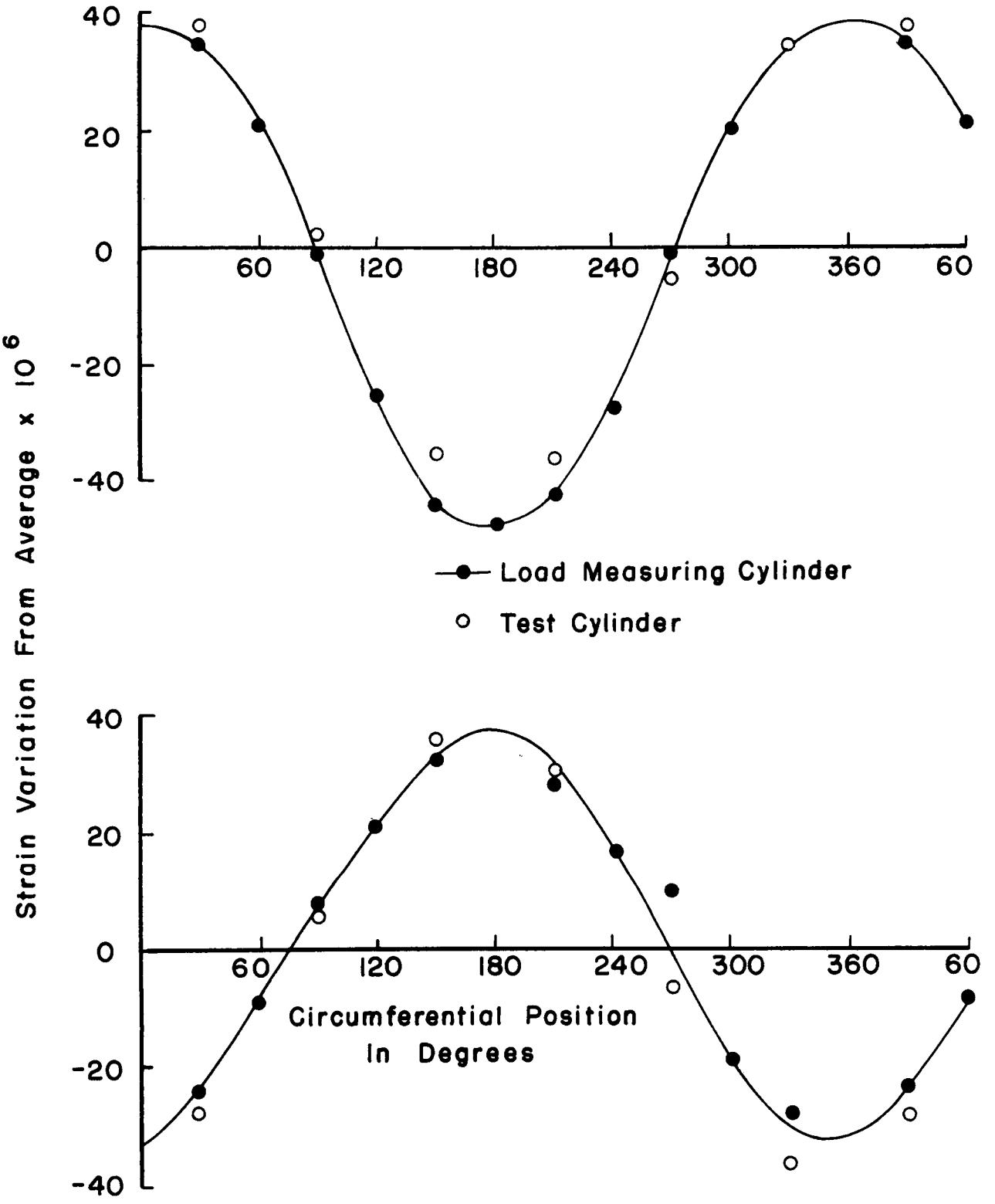

FIG. 6 - COMPARISON OF STRAIN IN TEST CYLINDER AND IN LOAD MEASURING CYLINDER

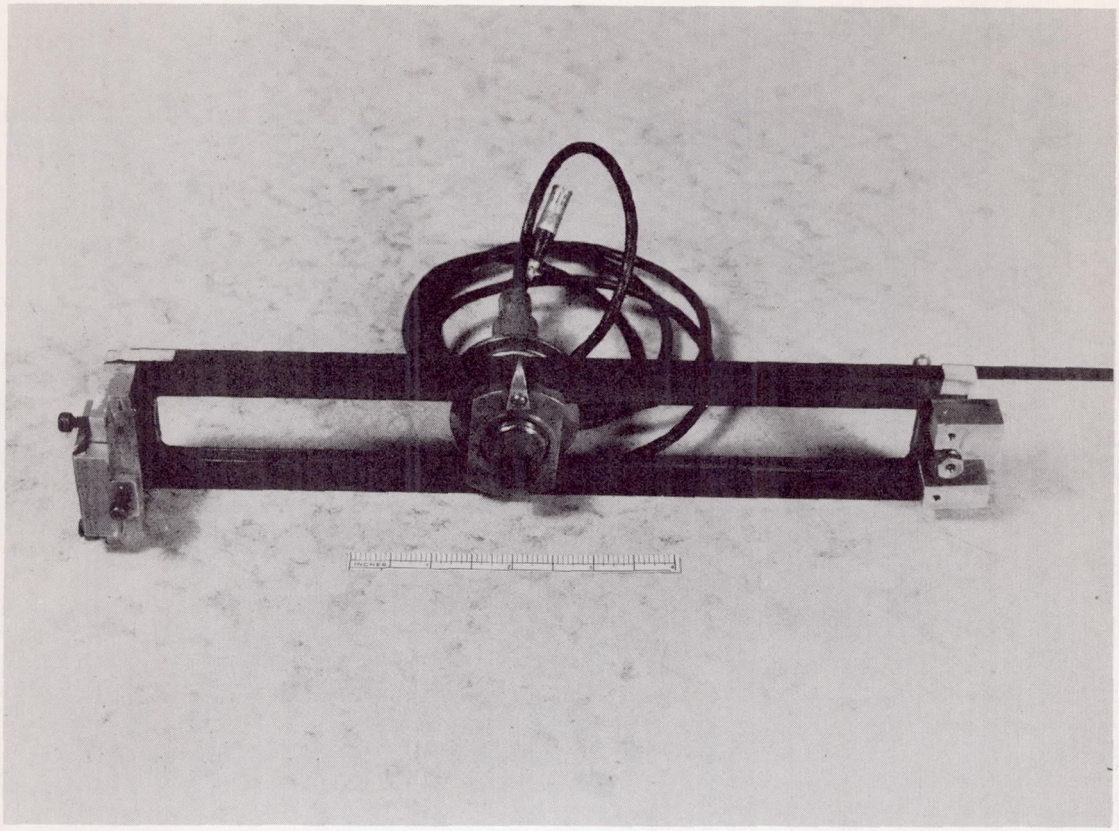

Fig. 7 - Initial Imperfection Measuring Equipment

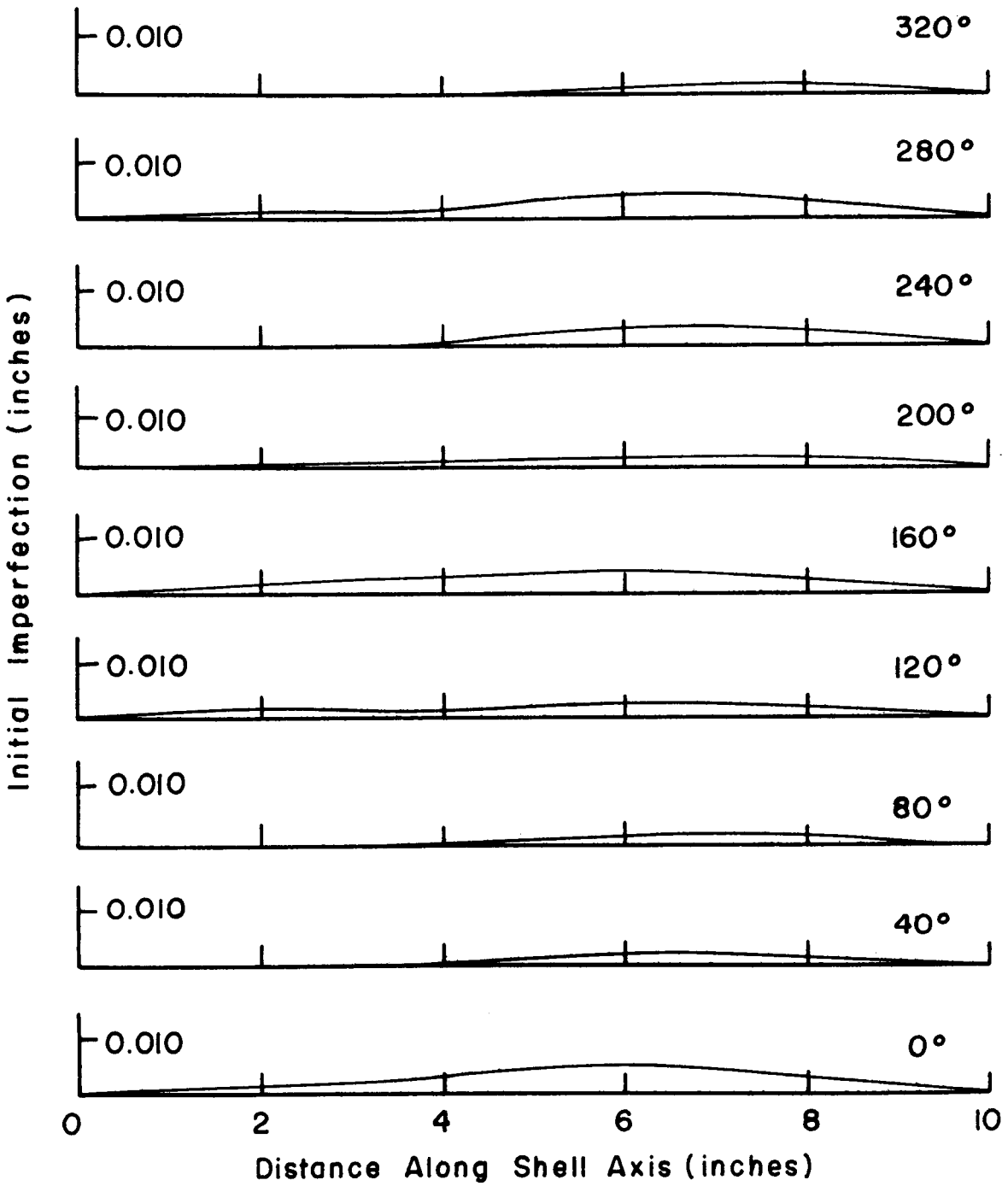

FIG. 8 - SHELL C INITIAL IMPERFECTION

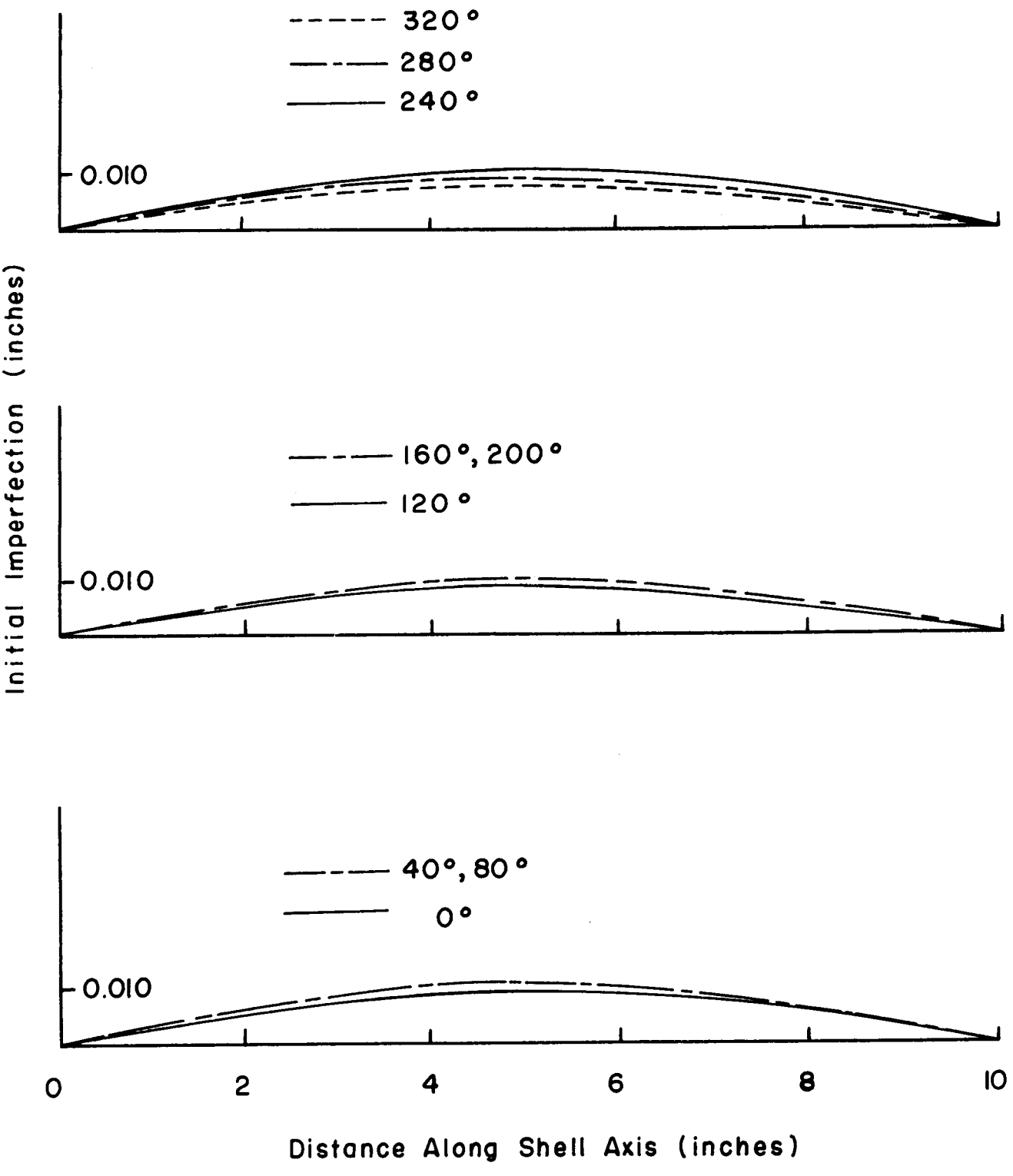

FIG. 9 - SHELL 7 INITIAL IMPERFECTION

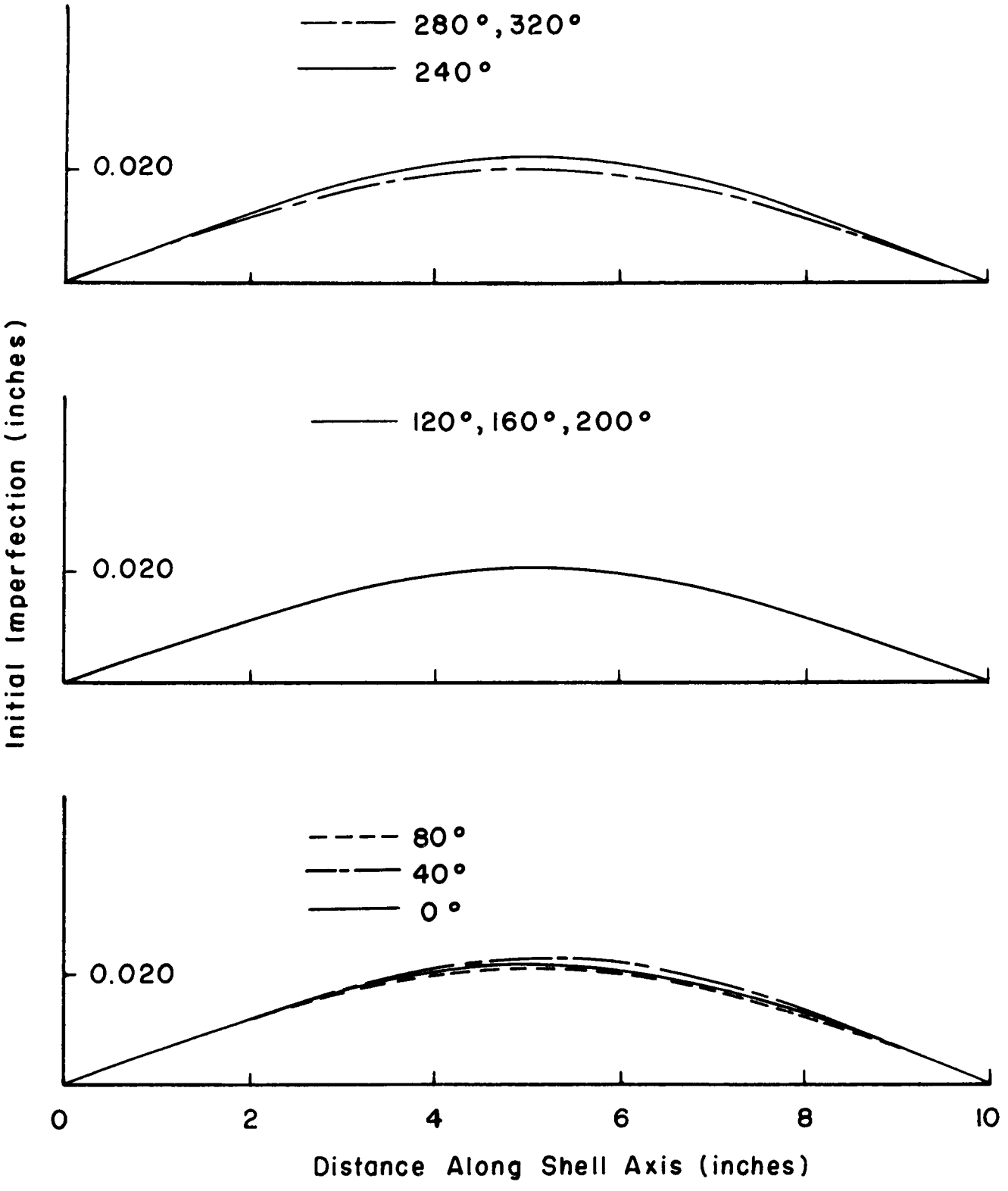

FIG. 10 - SHELL X INITIAL IMPERFECTION

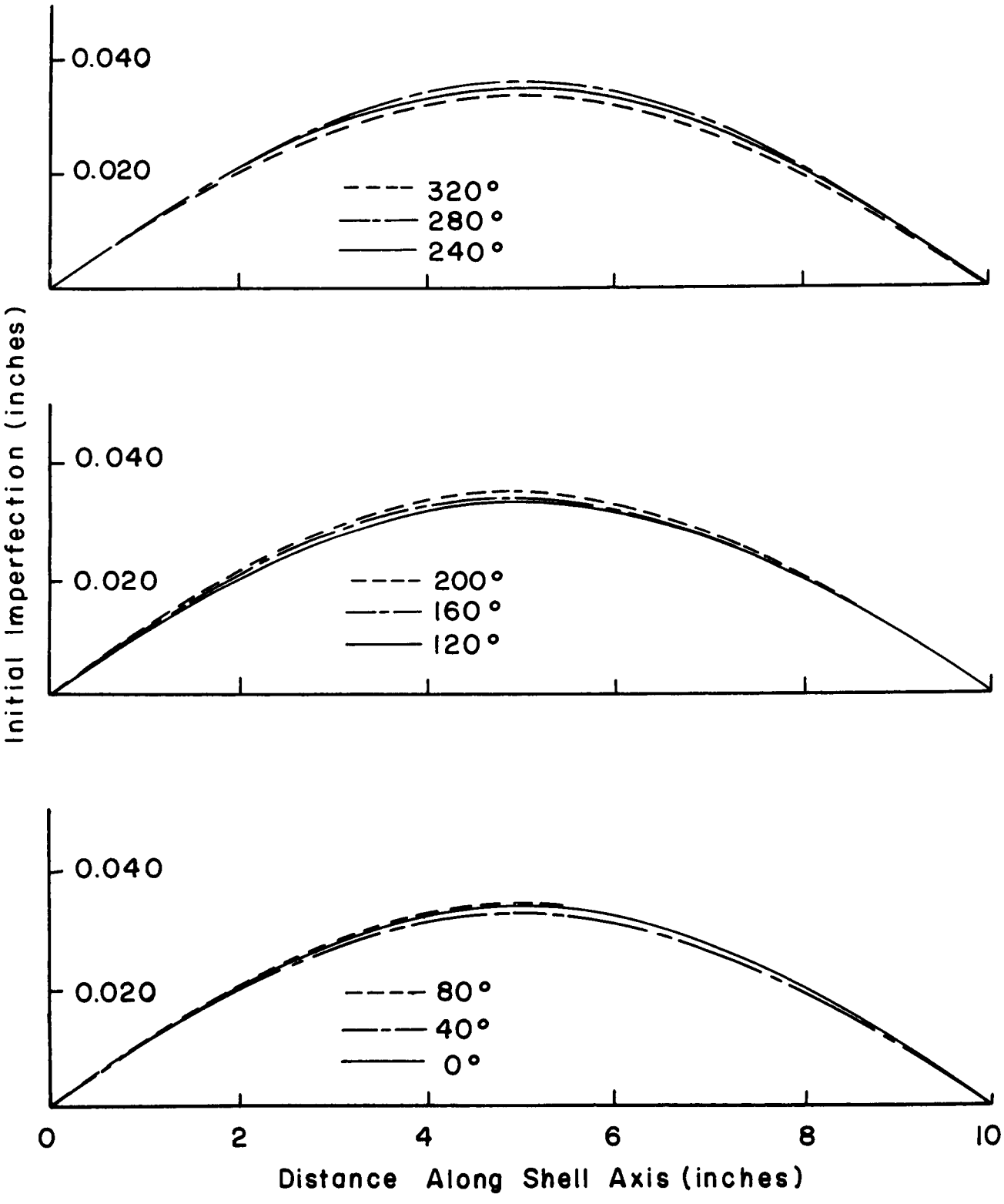

FIG. 11 - SHELL N INITIAL IMPERFECTION

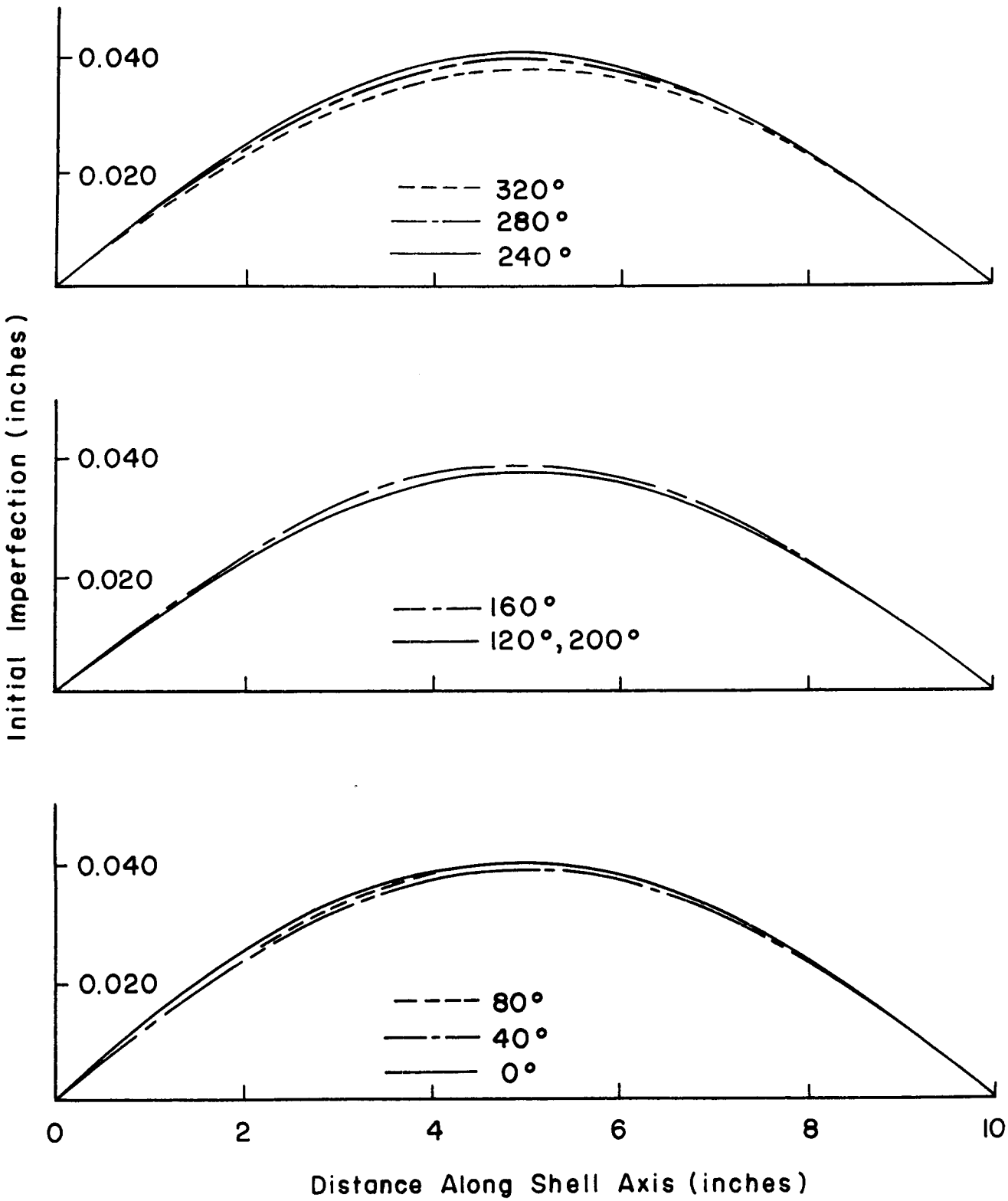

FIG. 12 – SHELL K INITIAL IMPERFECTION

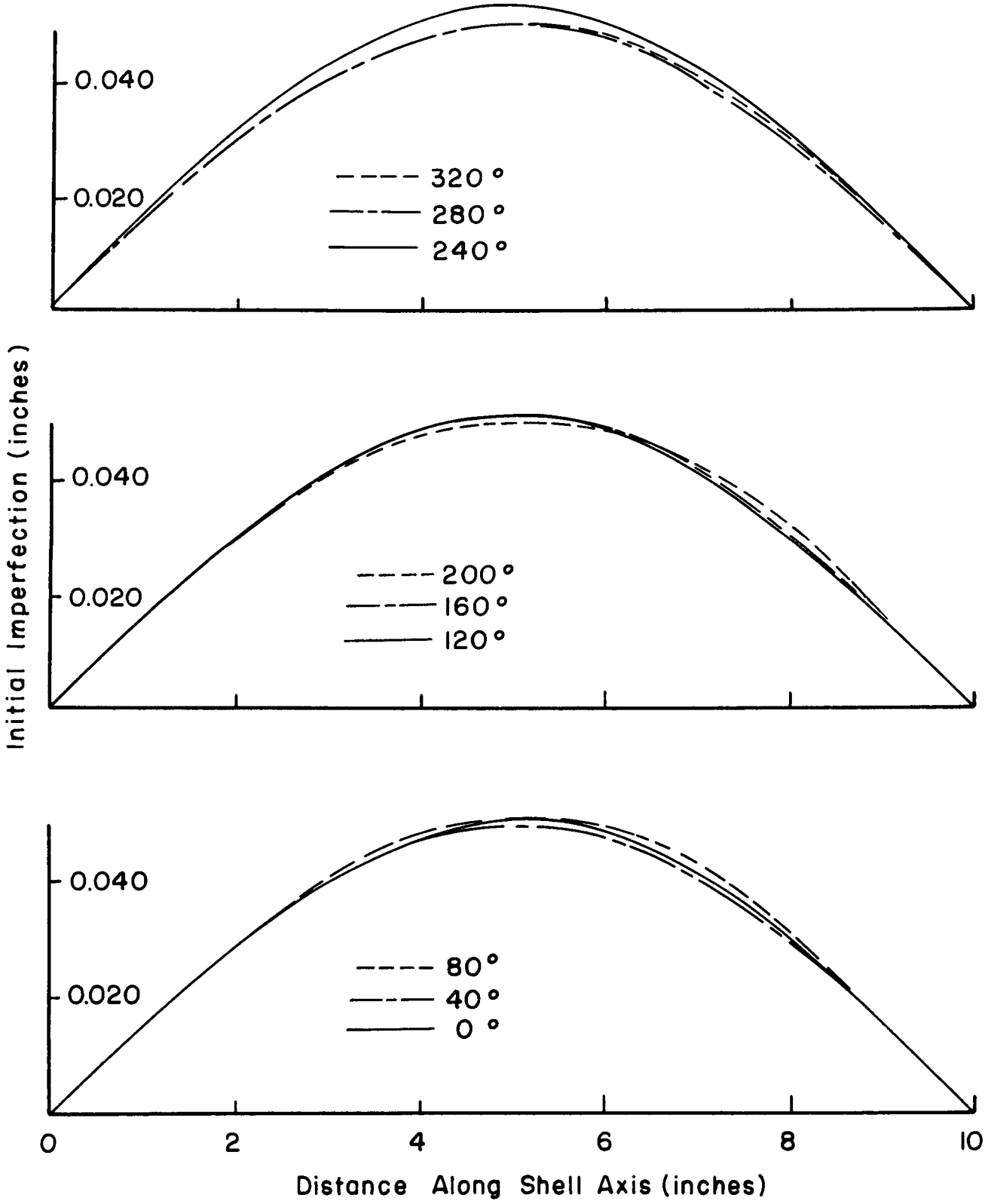

FIG. 13- SHELL G INITIAL IMPERFECTION

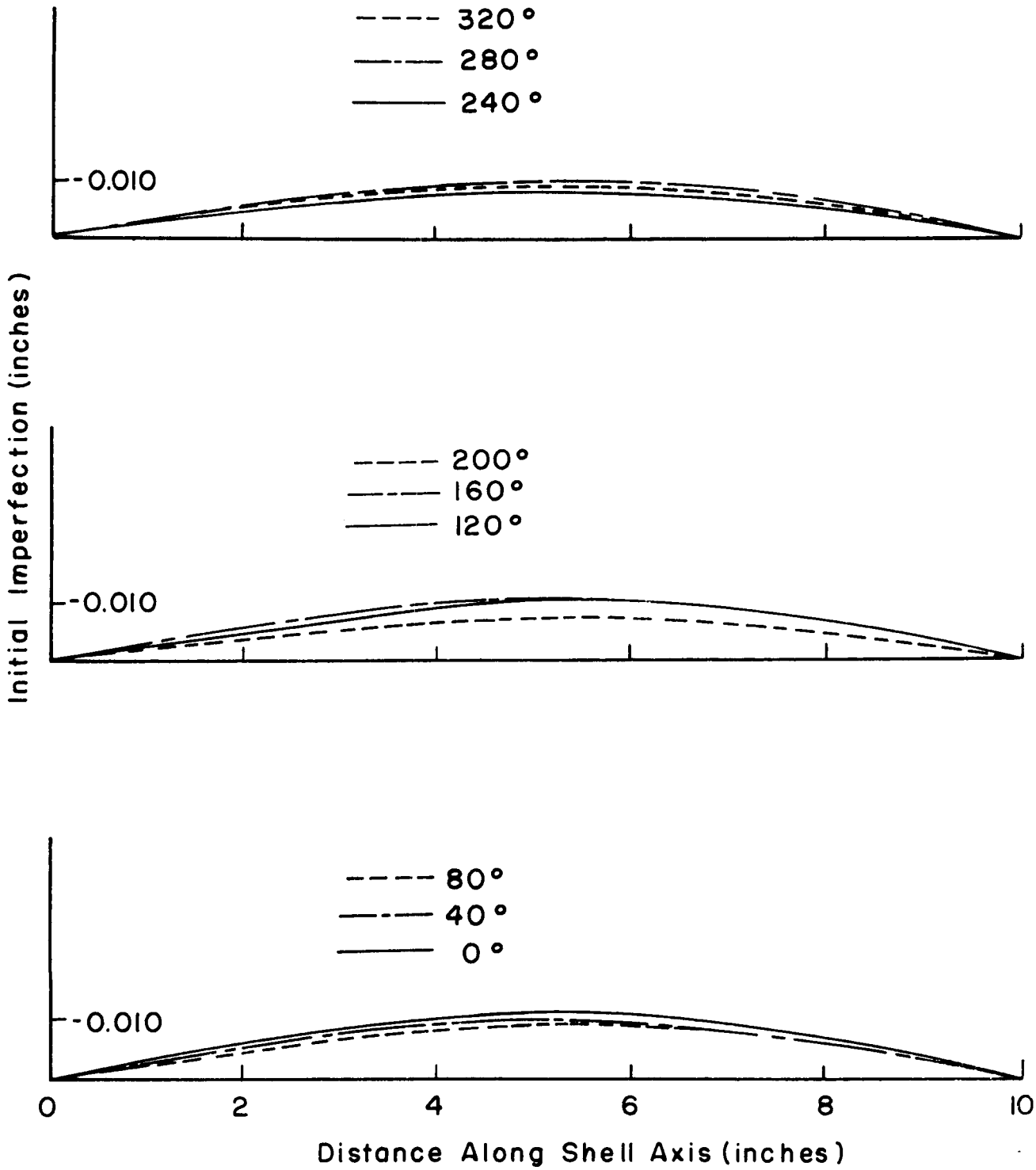

FIG. 14 - SHELL AD INITIAL IMPERFECTION

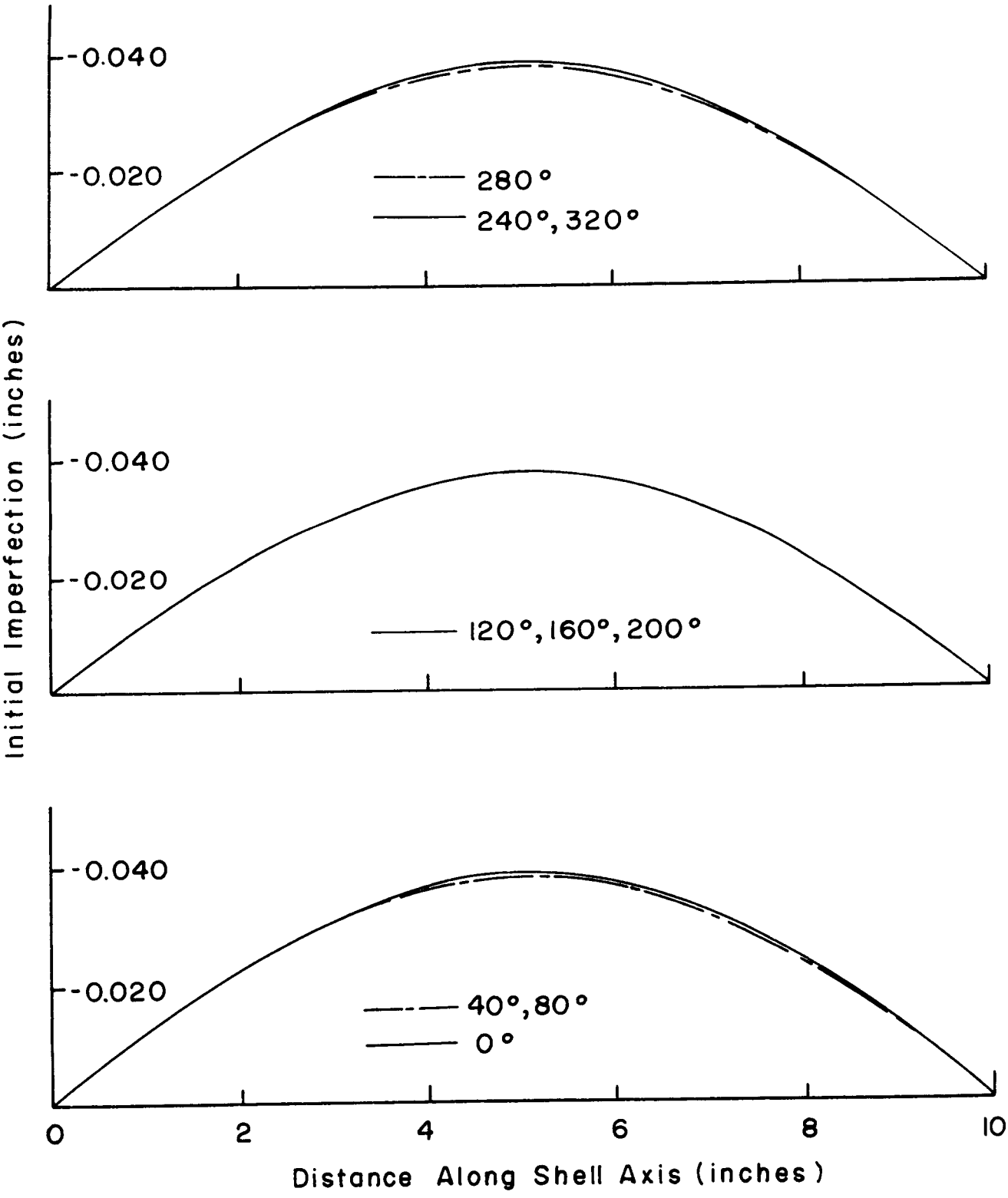

FIG. 15 - SHELL S INITIAL IMPERFECTION

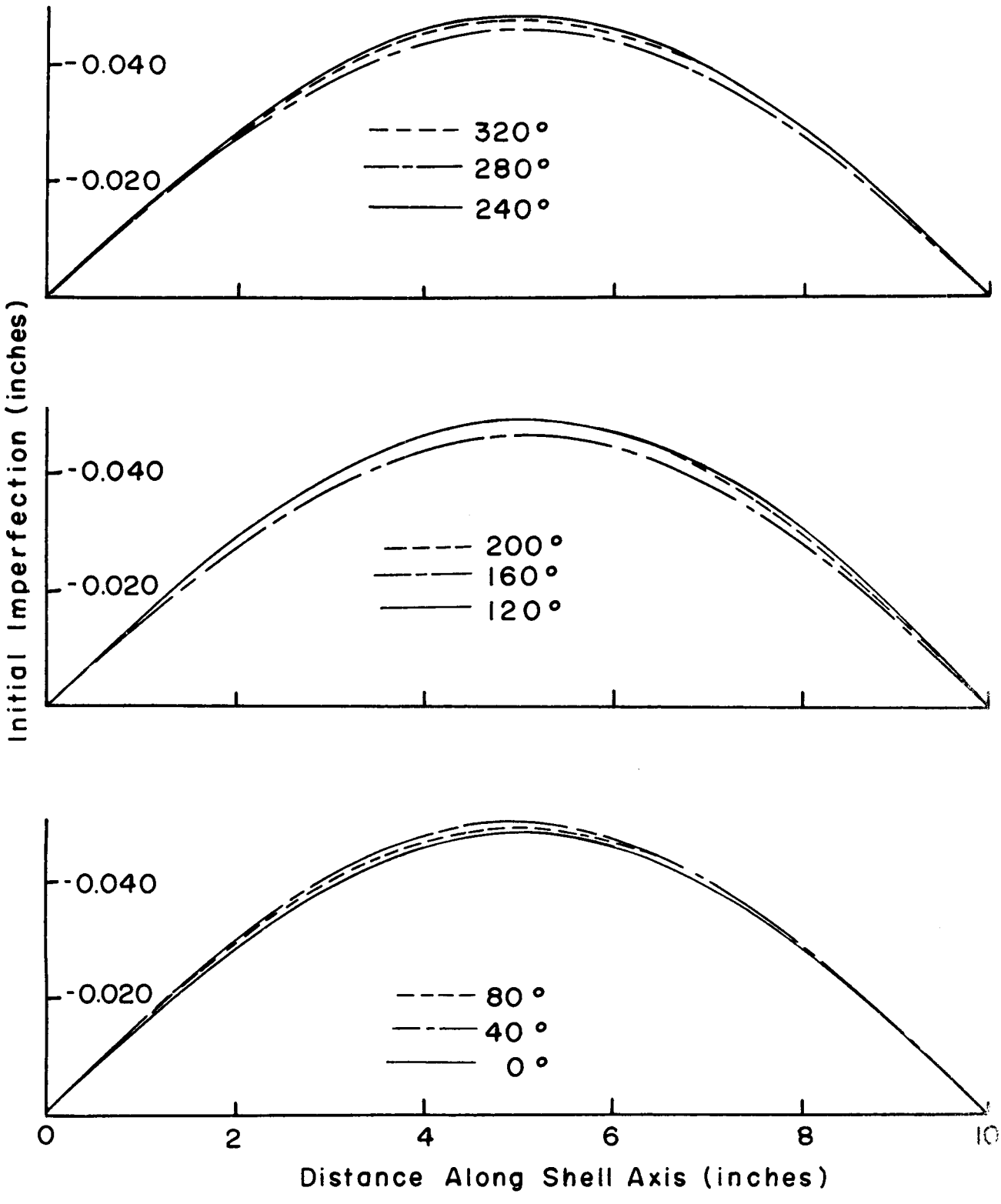

FIG. 16- SHELL R INITIAL IMPERFECTION

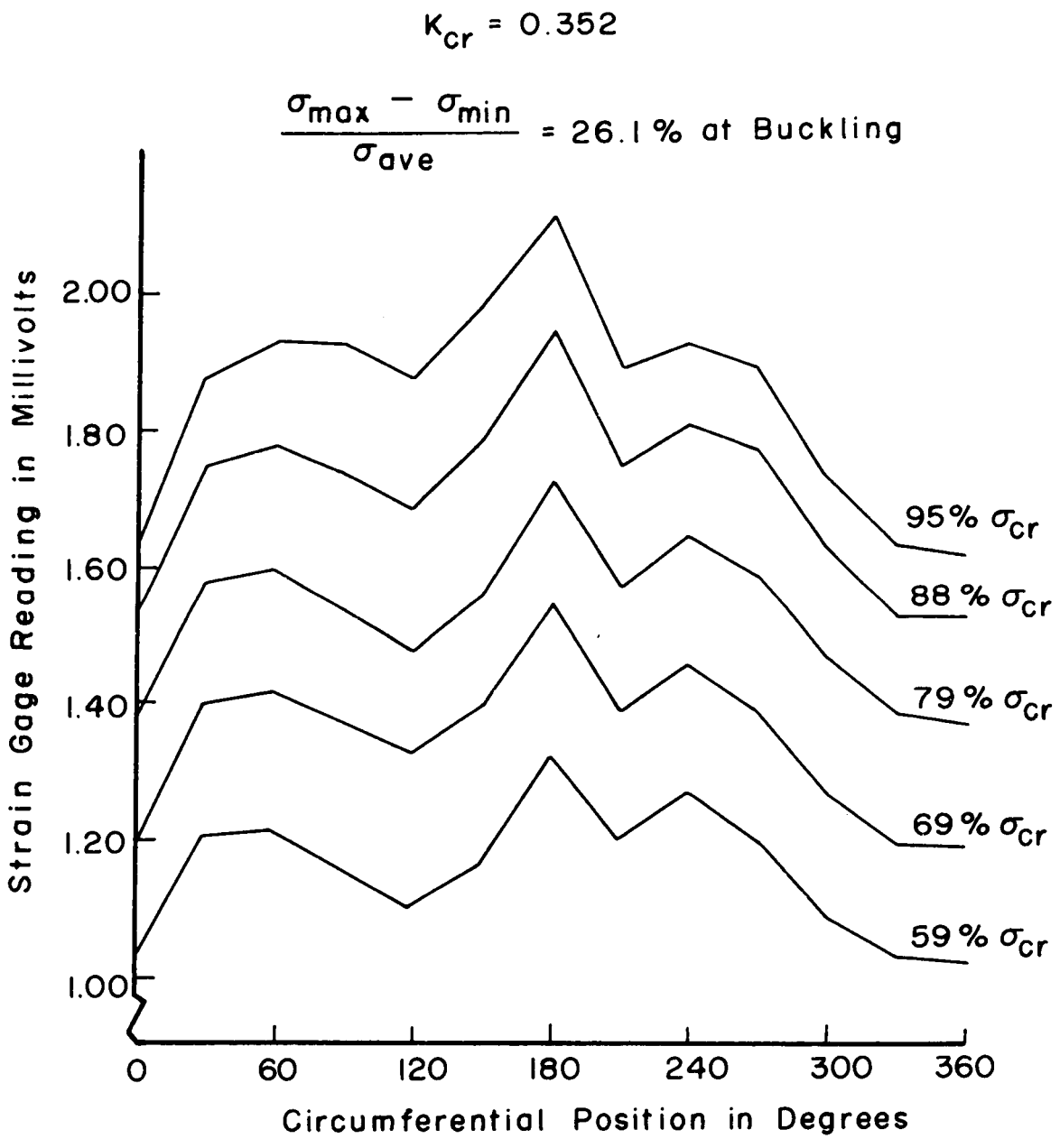

FIG. 17 - SHELL W LOAD DISTRIBUTION

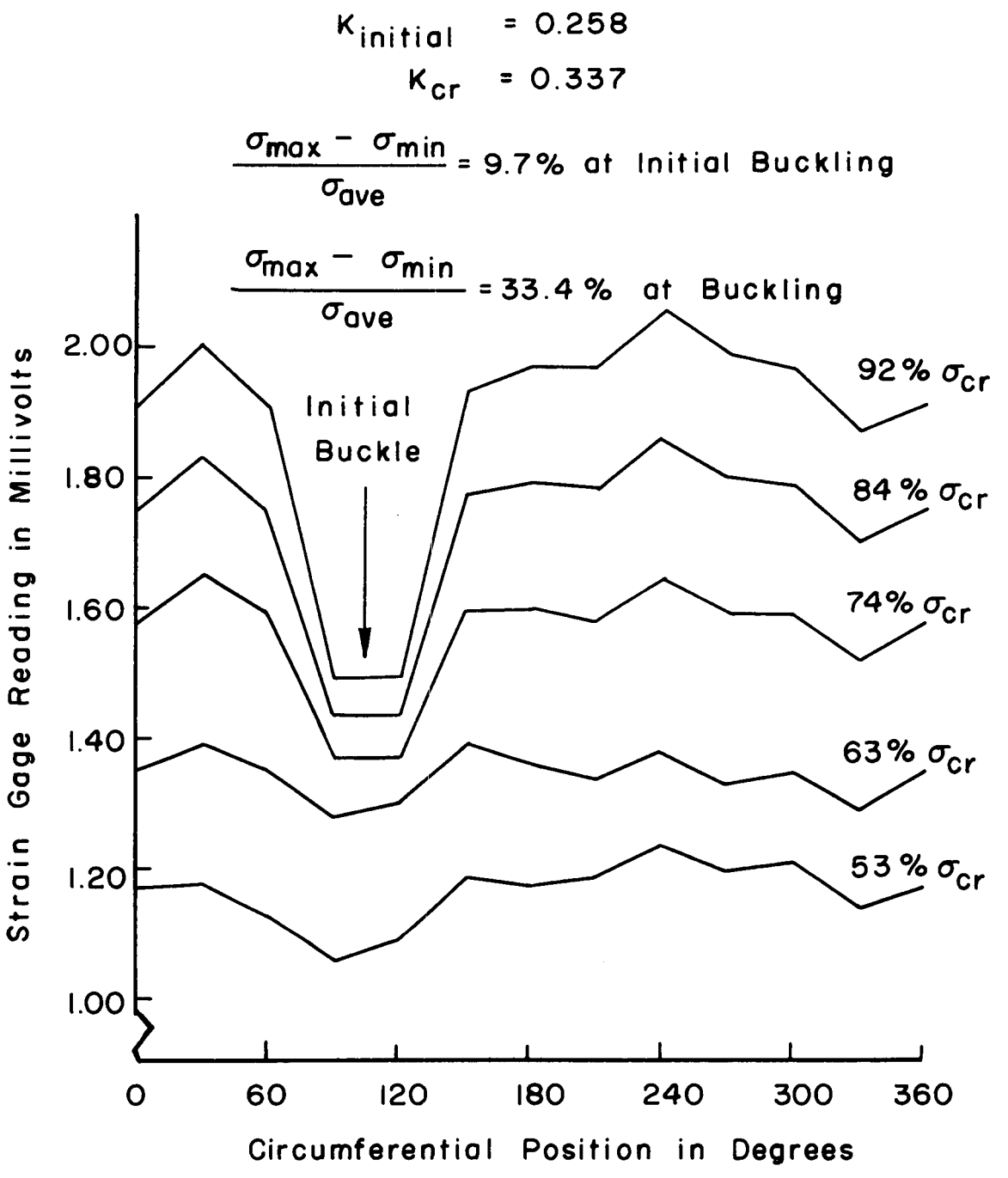

FIG. 18 - SHELL X LOAD DISTRIBUTION

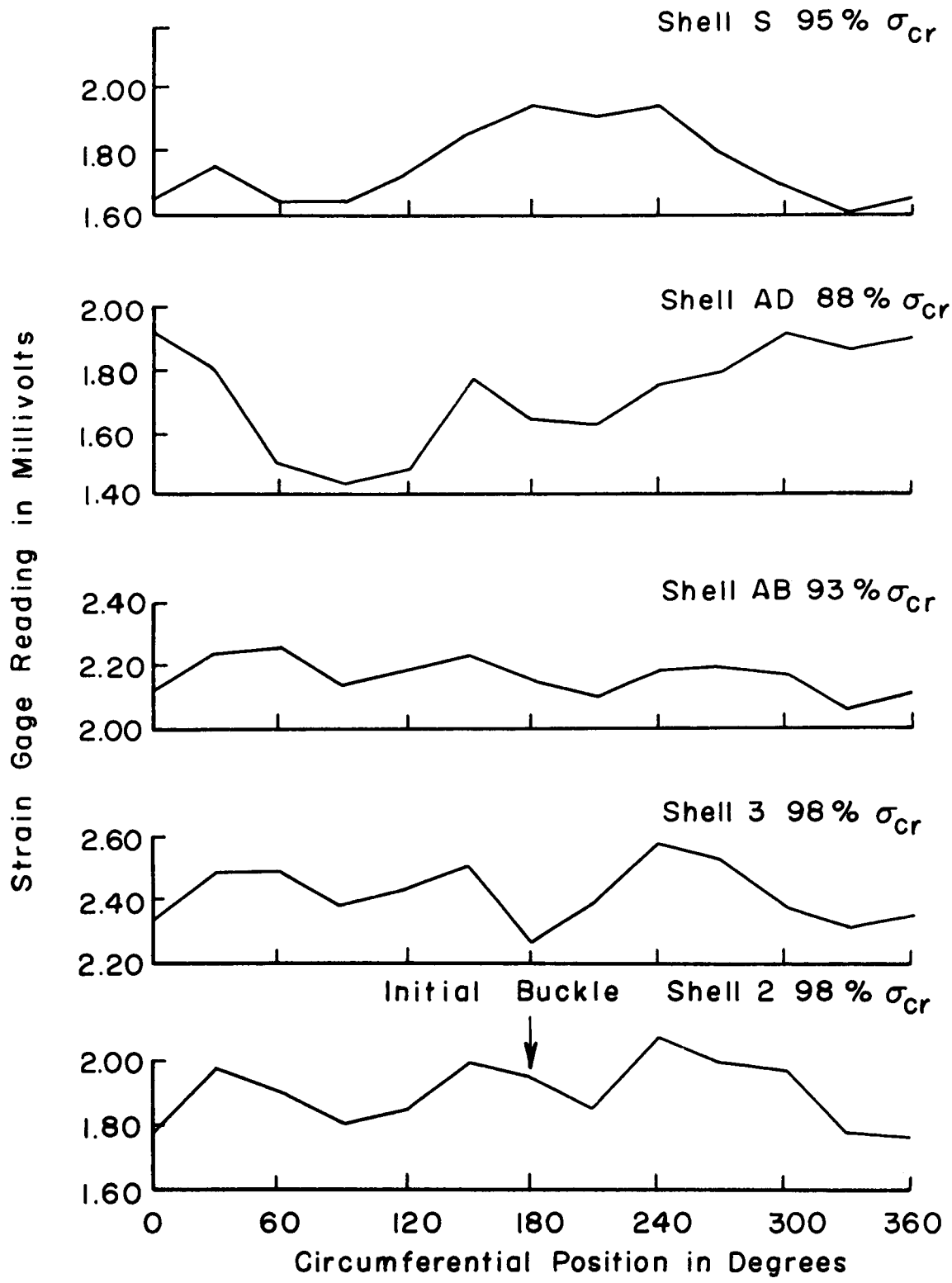

FIG. 19 - LOAD DISTRIBUTION NEAR BUCKLING SHELLS 2,3, AB, AD, S

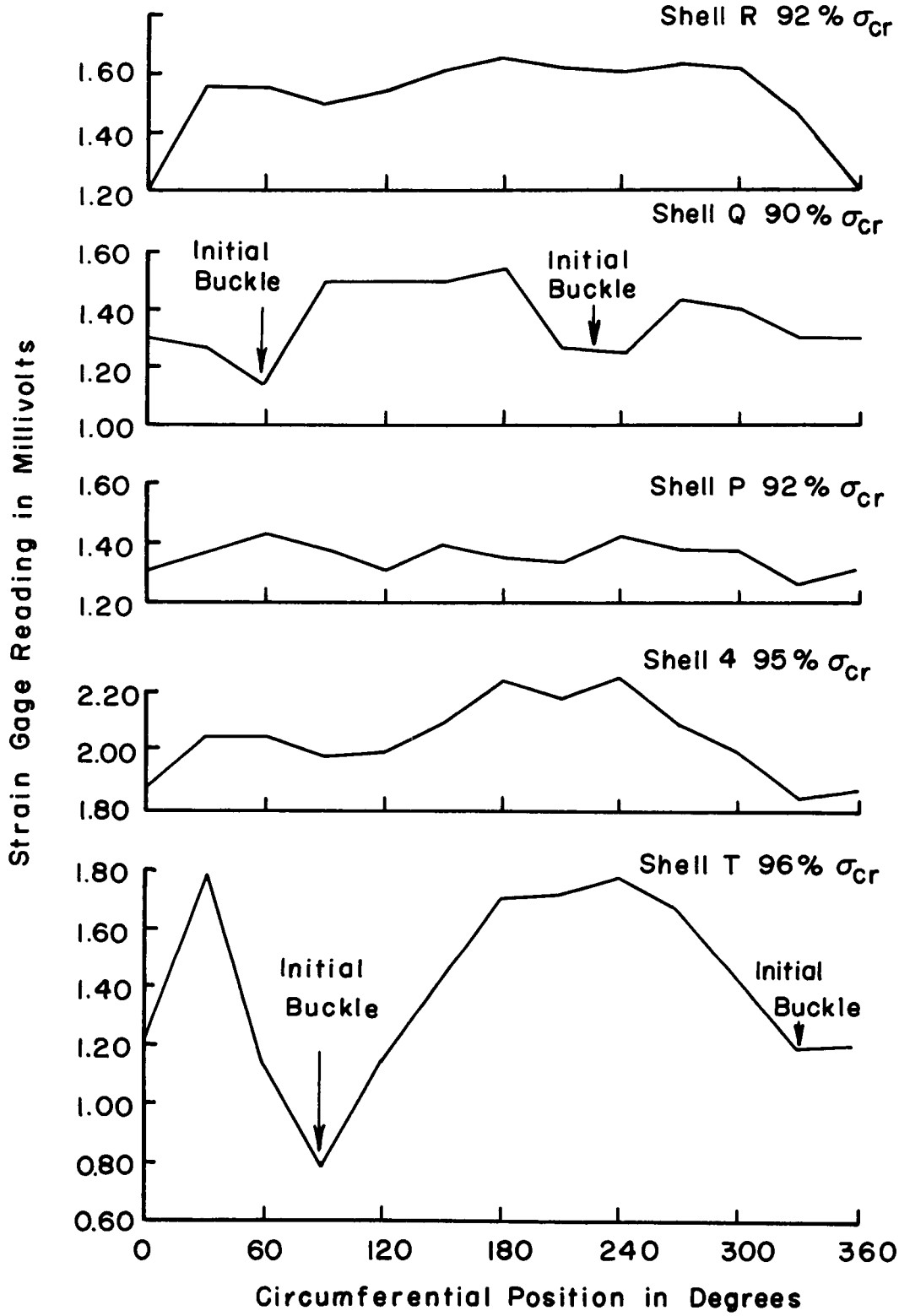

FIG. 20 - LOAD DISTRIBUTION NEAR BUCKLING SHELLS T, 4, P, Q, R

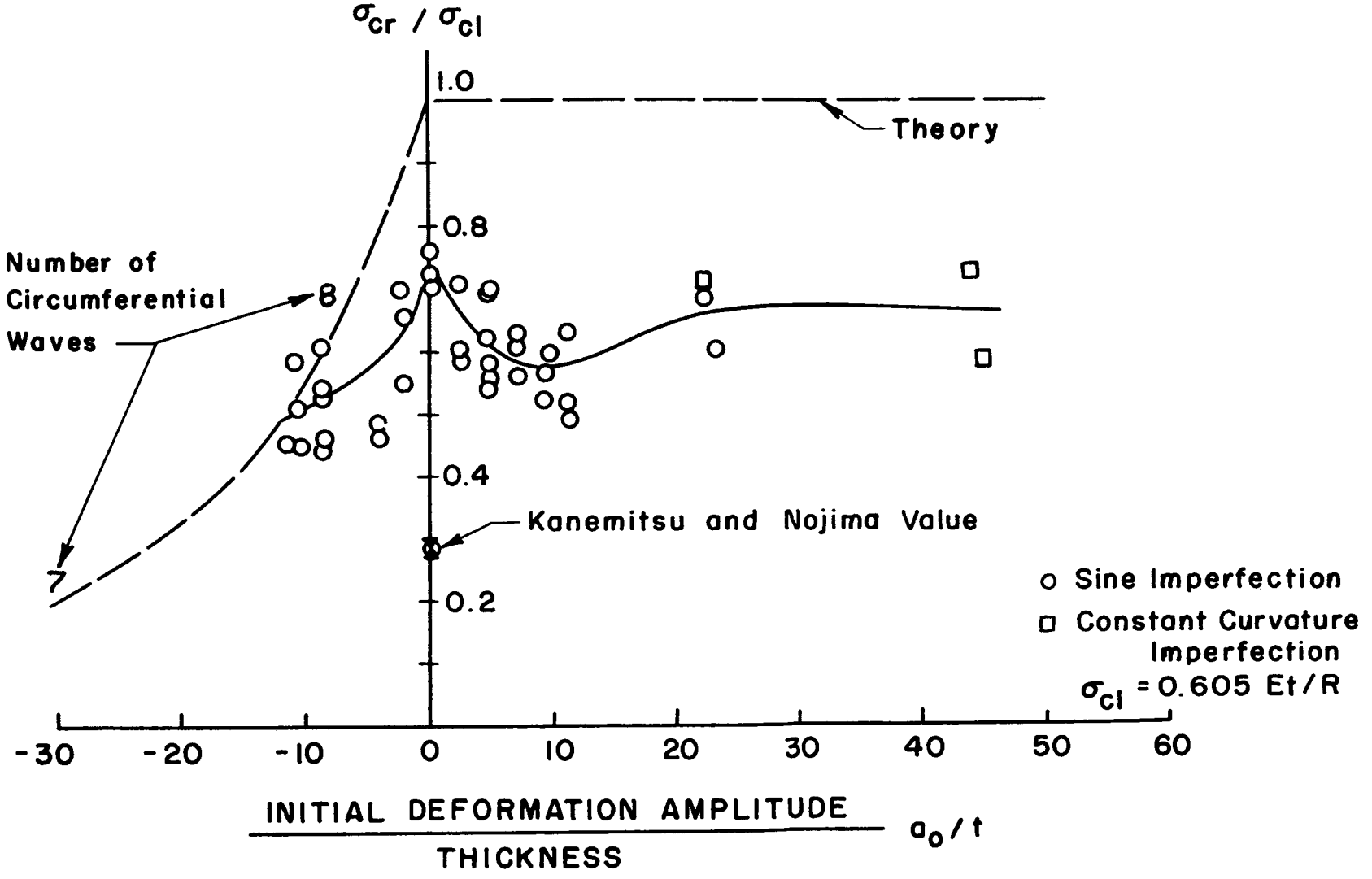

FIG. 21- BUCKLING STRESS VARIATION WITH INITIAL IMPERFECTION AMPLITUDE

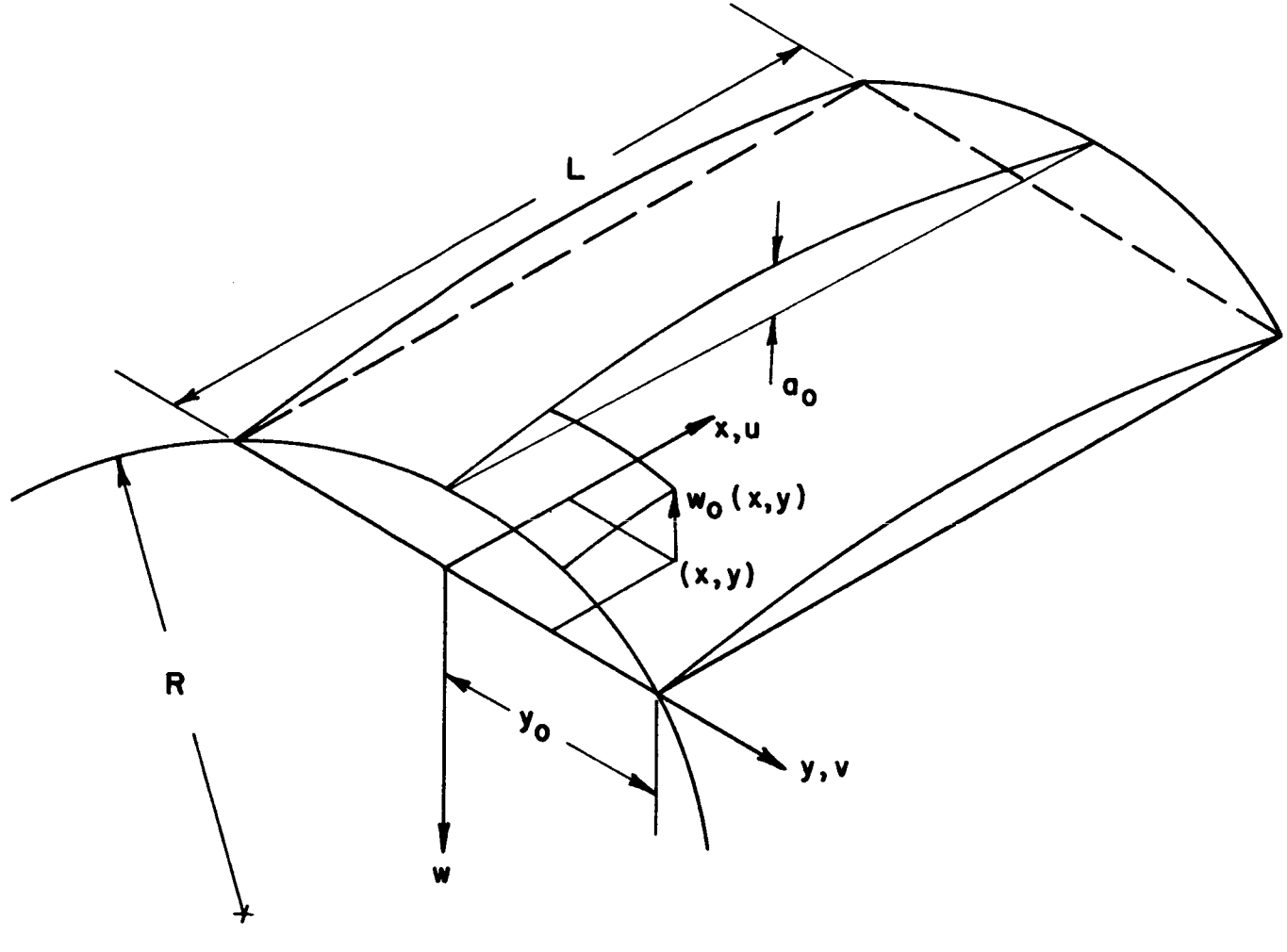

FIG. 22 – W_o FOR A CYLINDER WITH A HALF SINE WAVE INITIAL IMPERFECTION IN THE LENGTH DIRECTION

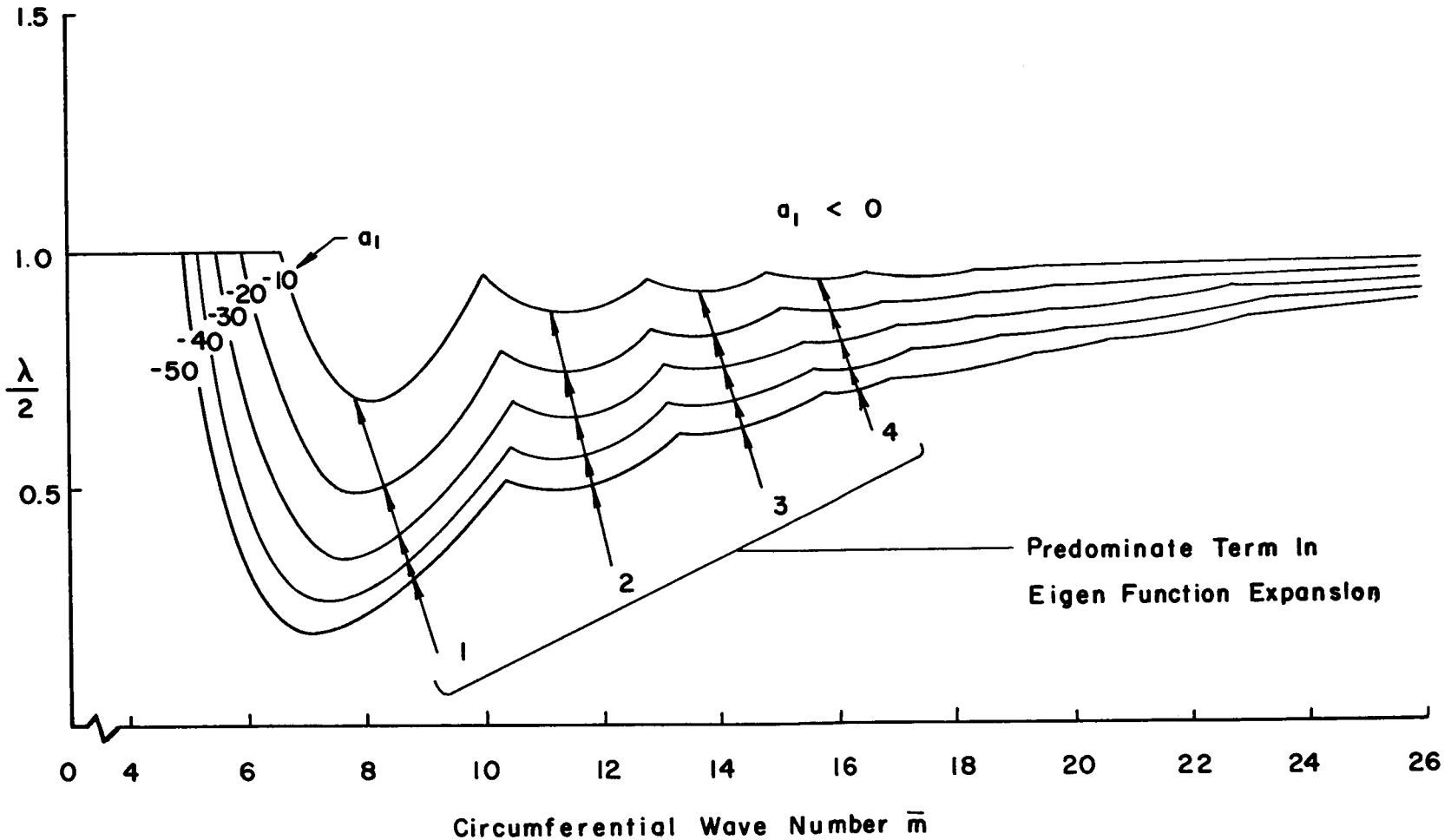

FIG. 23 - MINIMUM EIGEN VALUE VARIATION WITH THE CIRCUMFERENTIAL WAVE NUMBER

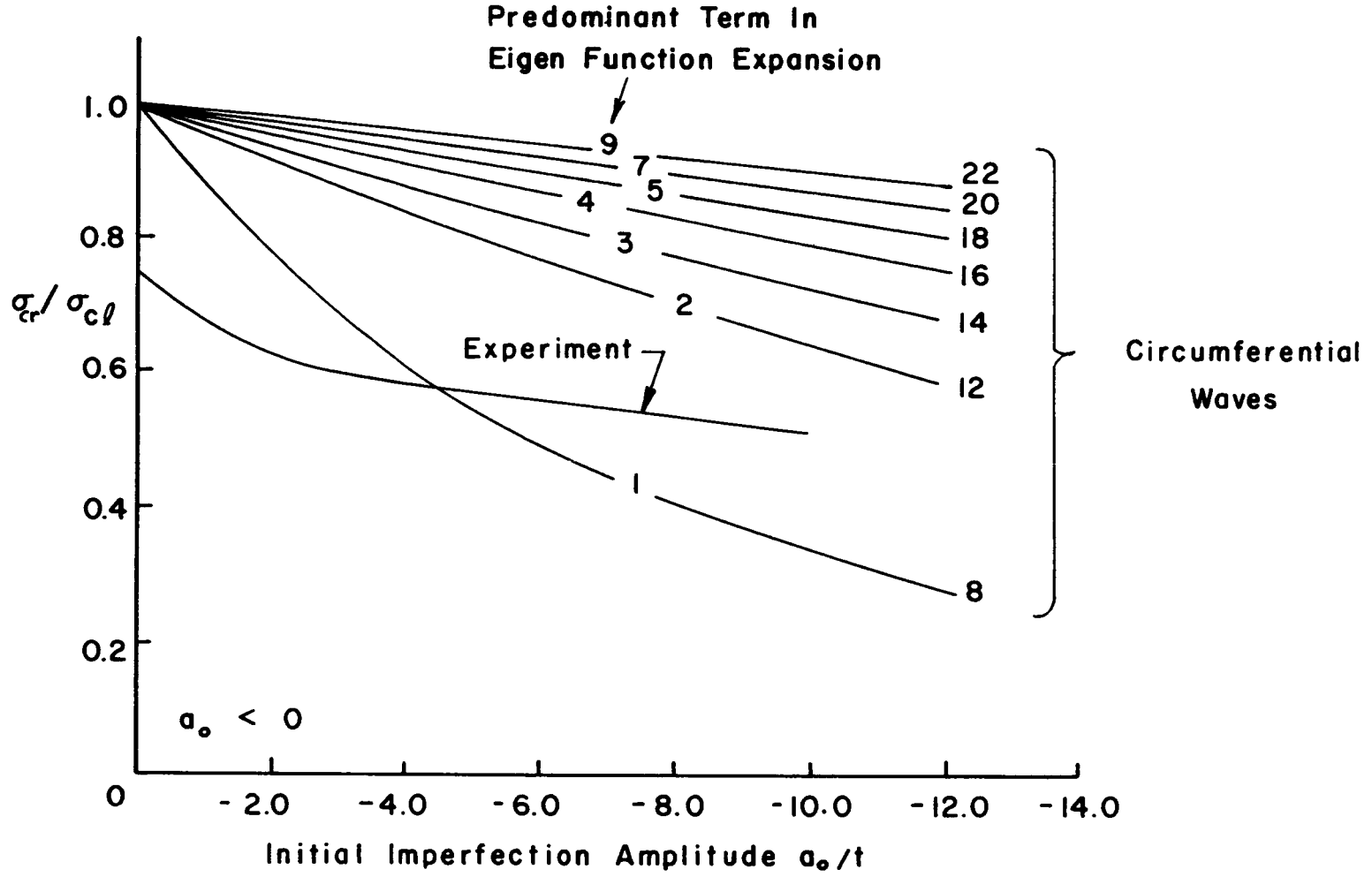

FIG. 24 - VARIATION OF BUCKLING STRESS WITH INITIAL IMPERFECTION AMPLITUDE AND CIRCUMFERENTIAL WAVE NUMBER